The Canadian Mineralogist
Vol. 44, pp. 667-692 (2006)

THE BEHAVIOR OF RARE-EARTH AND LITHOPHILE TRACE ELEMENTS IN RARE-METAL GRANITES: A STUDY OF FLUORITE, MELT INCLUSIONS AND HOST ROCKS FROM THE KHANGILAY COMPLEX, TRANSBAIKALIA, RUSSIA

ELENA V. BADANINA[§]

Geochemistry Department, St. Petersburg State University, Universitetskaja Emb. 7/9, St. Petersburg 199034, Russia

ROBERT B. TRUMBULL[¶]

GeoForschungsZentrum Potsdam, Sektion 4.2, Telegrafenberg, D-14473 Potsdam, Germany

PETER DULSKI

GeoForschungsZentrum Potsdam, Sektion 3.3, Telegrafenberg, D-14473 Potsdam, Germany

MICHAEL WIEDENBECK AND ILYA V. VEKSLER

GeoForschungsZentrum Potsdam, Sektion 4.2, Telegrafenberg, D-14473 Potsdam, Germany

LUDMILA F. SYRITSO

Scientific Research Institute of Earth Crust, St. Petersburg State University, St.Petersburg 199034, Russia

ABSTRACT

We have determined trace-element concentrations in fluorite mineral separates, host granites and residual melts trapped in quartz from a well-documented sequence of differentiated Li–F-rich granites in the Khangilay complex, Transbaikalia, Russia, which are associated with Ta (Orlovka) and W (Spokojnoje) mineralization. Fluorite is a common accessory mineral in most units of the granite sequence and in greisen veins from their hydrothermal aureoles. This allows us to monitor the behavior of REE and other fluorite-compatible trace elements during the magma evolution, and to compare magmatic and hydrothermal REE signatures directly. With increasing differentiation of the granites, REE abundances decrease, chondrite-normalized patterns become flat, and negative Eu anomalies more pronounced. Fluorite separates from the respective granites show similar REE patterns and 5–10 times higher concentrations (up to 4000 ppm total REE). First-order features of the whole-rock, fluorite and melt-inclusion REE characteristics are the presence of extreme negative Eu anomalies and the strong lanthanide tetrad effects in the more evolved units. Samples with the tetrad effect also show strong separation of geochemical twin elements (Y–Ho, Zr–Hf). Although melt-inclusion data prove that the lanthanide tetrad effect developed during the magmatic stage, the process cannot be explained by simple fractional crystallization. Partitioning of REE to a F-bearing hydrothermal solution also is unlikely because hydrothermal fluorite from associated veins and greisen does not show complementary W-tetrads. We suggest that the tetrad effect and deviations of element ratios observed in this and other highly evolved F-rich granites are caused by separation of a F-rich hydrosaline melt. This is consistent with results of experimental partitioning studies of immiscible silicate and hydrosaline melts.

Keywords: melt inclusions, tetrad effect, rare-earth elements, fluorite, rare-metal granites, hydrosaline melt, immiscibility, secondary-ion mass spectrometry, Orlovka, Spokojnoje, Transbaikalia, Russia.

SOMMAIRE

Nous avons établi la concentration d'éléments traces dans des concentrés de fluorite, le granite hôte, et des reliquats magmatiques piégés dans le quartz provenant de séquences bien différenciées de granites enrichis en Li–F du complexe de Khangilay, en Transbaïkalie, Russie, qui sont associées à une minéralisation en Ta (Orlovka) et W (Spokojnoje). La fluorite est un accessoire commun dans la plupart des unités intrusives et dans les greisen et les veines hydrothermales de leurs aureoles hydrothermales. C'est ce qui nous permet de contrôler le comportement des terres rares et autres éléments traces compatibles avec la fluorite au

§ *E-mail address*: lena@lenusik.usr.pu.ru
¶ *E-mail address*: bobby@gfz-potsdam.de

cours de l'évolution du magma, et de comparer les signatures magmatique et hydrothermale de ses comportements directement. A mesure que progresse la différenciation de ces granites, les teneurs en terres rares diminuent, les tracés de concentrations normalisés par rapport à une chondrite deviennent plats, et une anomalie négative en Eu devient plus prononcée. Les concentrés de fluorite des granites respectifs montrent des tracés de concentration de terres rares semblables et des concentrations de 5 à 10 fois plus fortes (jusqu'à un total de 4000 ppm). Les aspects de premier ordre des terres rares des roches totales, de la fluorite et des inclusions vitreuses sont la présence d'anomalies négatives extrêmes en Eu et de fortes expressions de l'effet de tétrades parmi les terres rares dans les unités les plus évoluées. Les échantillons montrant l'effet de tétrades aussi font preuve d'une forte séparation des éléments géochimiquement jumelés (Y–Ho, Zr–Hf). Quoique les données sur les inclusions vitreuses prouvent que l'effet tétrade parmi les terres rares s'est développé au cours du stade magmatique, on ne peut expliquer le processus simplement par cristallisation fractionnée. Une répartition des terres rares en faveur d'une solution hydrothermale fluorée aussi semble peu probable parce que la fluorite hydrothermale des veines et greisens associés ne montrent pas un développement complémentaire de tétrades en forme de W. Nous croyons que l'effet de tétrade et les déviations des rapports d'éléments observés, ici et dans d'autres granites riches en fluor et fortement évolués, résultent de la séparation d'un liquide riche en fluor et hydrosalin. Cette hypothèse concorderait avec les résultats expérimentaux portant sur la répartition d'éléments entre fractions liquides silicatée et hydrosaline immiscibles.

(Traduit par la Rédaction)

Mots-clés: inclusions vitreuses, effet tétrade, terres rares, fluorite, granites enrichis en métaux rares, liquide hydrosalin, immiscibilité, spectrométrie de masse des ions secondaires, Orlovka, Spokojnoje, Transbaïkalie, Russie.

Introduction

The processes responsible for element transport and mineralization in volatile-rich silicic magmas at low pressure, where exsolution of one or more fluid phases can be expected to play a key role, are highly complex and still not well understood despite decades of research (*e.g.*, Jahns & Burnham 1969, Luth & Tuttle 1969, Burnham 1979, Beus 1982, Černý 1982, Pollard 1986, London *et al.* 1988, Candela 1990, London 1992, Keppler 1993, Raimbault *et al.* 1995, Salvi & Williams-Jones 1996, Linnen 1998, Audétat *et al.* 2000, Thomas *et al.* 2000, 2005). In this paper, we discuss recent progress toward understanding the economically important class of Li–F-rich, rare-metal granites, based on new studies of one of its best-known examples: the Khangilay complex of eastern Transbaikalia. Previous investigators suggested that some features of the late-stage units in the Orlovka subintrusion required interaction with a separate comagmatic or postmagmatic fluid phase (Beskin *et al.* 1994, Syritso *et al.* 2001). However, the nature of these processes and the fluid responsible could not be specified from the available evidence. The studies of fluid and melt inclusions by Reyf *et al.* (2000) and Badanina *et al.* (2004) provided important information on the composition of residual melts and inferred magmatic fluid(s). A key finding of the latter study was that Na–K–Al variations in melt inclusions from the most evolved Orlovka units suggest unmixing of a Na–F-rich magmatic fluid (hydrosaline melt).

In this contribution, we further characterize the roles of melt- and fluid-based processes in the late-stage evolution of the Khangilay granites using trace-element data. The focus is on the rare-earth elements (REE) and Y because much is known about their behavior in igneous and hydrothermal systems, and their use for petrogenetic interpretation is well established. Of special importance for mineralized granites is the suggestion that distinctive features of REE distribution patterns and specific element ratios (*e.g.*, the tetrad effect, Y:Ho ratio: Bau 1996, 1997) may be diagnostic of fluid–melt rather than crystal–melt partitioning, a topic discussed extensively in this paper. Despite their potential importance, the REE in the Khangilay granites have not previously been studied in detail. Our work is based on new bulk analyses of whole-rock samples and fluorite separates that cover the full range of internal units in the intrusions, supplemented by *in situ* analyses of individual quartz-hosted melt inclusions from the most highly evolved units in the Orlovka subintrusion. We also analyzed fluorite from greisen bodies and quartz veins in the endo- and exocontacts to monitor the behavior of the REE in the hydrothermal aureoles of the granites. Fluorite is an excellent monitor of REE behavior because it is relatively common in both magmatic and hydrothermal environments and a favorable host for the rare-earth elements, Y and Sr, which substitute for Ca (Grappin *et al.* 1979, Strong *et al.* 1984, Jebrak *et al.* 1985, Constantopoulos 1988, Ivanova *et al.* 1995, Bau & Dulski 1995, Kuprianova *et al.* 2002, Bau *et al.* 2003). There have been relatively few applications of REE data on fluorite in granitic systems compared with hydrothermal studies. Part of the reason may be the perception that fluorite in granites is a secondary mineral. However, magmatic fluorite occurs as a phenocryst phase in felsic volcanic rocks (Marshall *et al.* 1998), and its presence has been inferred in several granites from petrographic evidence (*e.g.*, Bailey 1977, Price *et al.* 1999, Dolejš & Stemprok 2001). Scaillet & Macdonald (2001, 2004) described magmatic crystallization of fluorite in experimental studies with peralkaline granitic compositions, and a thermodynamic analysis by Dolejš & Baker (2004)

demonstrated fluorite stability in common compositions of both peralkaline and peraluminous granitic magmas. As we show below, the fluorite from granites in the Orlovka and Spokojnoje intrusion is dominantly magmatic.

Regional Setting and Geology of the Khangilay Granites

The Khangilay massif is situated in the central part of the Paleozoic Aginsk block of Eastern Transbaikalia (Zanvilevich *et al*. 1985). The shallow-level intrusion of Jurassic age (142.9 ± 0.9 Ma: Negrey *et al*. 1995, Kovalenko *et al*. 1999) consists, at the surface, of biotite or two-mica granites and two satellite intrusions of mineralized granites, Orlovka and Spokojnoje (Fig. 1). The country rocks comprise a heterogeneous series of terrigenous, low-grade metasedimentary rocks (sandy phyllites, tuffaceous sandstones, siltstones, conglomerates with layers of metabasic rock, acid effusive rock and tuff). Hornfels is commonly developed in the country rocks at the intrusive contacts. In the vicinity of the Spokojnoje massif, the exocontact locally contains garnet-bearing skarn-like rocks and abundant muscovite–fluorite veins. The roof zone of this intrusion was intensely injected with granitic dikes and quartz veins, the latter including "wolframite" mineralization. Some exocontact rocks in this zone contain crusts of green fluorite that have replaced carbonate-rich lenses. These rocks are absent in the roof zone of the Orlovka

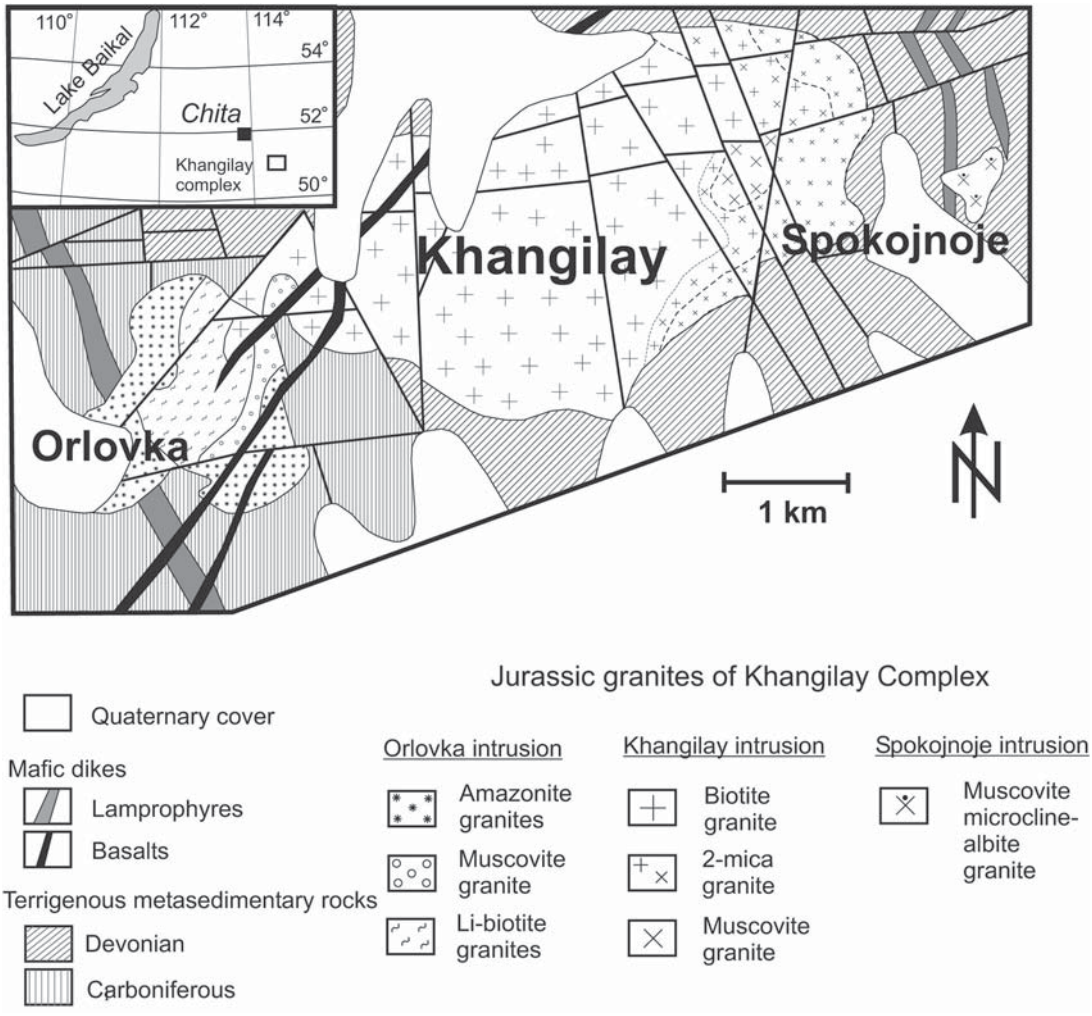

FIG. 1. Simplified geological map of the Khangilay granite complex in eastern Transbaikalia, modified from Syritso *et al*. (2001).

massif. Instead, dikes of fine-grained rare-metal granite and pegmatitic bodies of quartz–amazonitic K-feldspar with lepidolite occur, and there is a zone of intense greisenization with distinctive protolithionite–topaz greisen containing abundant beryl and pockets of color-zoned fluorite. One reason for the contrast between the roof zones of the two intrusive bodies may be the presence of flat-lying dikes of pre-granite lamprophyre up to 200 m thick above the Orlovka massif, which may have retarded the loss of magmatic volatiles. Several different types of igneous dikes are present in the Khangilay area (Fig. 1). Pre-granite dikes include lamprophyres, andesite porphyries and rhyolites. Later dikes that cut the Orlovka amazonitic K-feldspar granite have a subalkaline basaltic composition. A third group of dikes has more evolved granitic compositions (trachy-rhyolites and trachy-rhyodacites) and are perhaps related to the rare-metal granites. They are concentrated in the tectonically weak zone in the northwestern surroundings of the massif and have been studied by Syritso *et al*. (2005), who determined a Rb–Sr age of 139 ± 4 Ma, which is within error of the age of the Khangilay massif. The dikes share some of the geochemical specialization shown by the Orlovka massif, but differences in Sr and Nd isotope ratios rule out a direct genetic relationship (Syritso *et al*. 2005).

Details of the geology, mineralogy and whole-rock geochemistry of the Khangilay complex are given by Beskin *et al*. (1994), Syritso (1993) and Syritso *et al*. (2001). An overview of the main lithologic units is given in Table 1, and schematic profiles through the intrusions are shown in Figure 2. The Spokojnoje intrusion shows a relatively simple variation from the bottom upward, with muscovite granites to muscovite – microcline – albite granites and apical quartz–muscovite greisens containing W mineralization. Accessory minerals include fluorite, apatite, zircon, garnet (almandine–spessartine), ferberite and other tungstates ("chillagite", russellite and "hoongarrite"). The contents of fluorite increase rapidly upward in the granite and reach a maximum level in the greisen. Vertical zoning in the Orlovka massif is much better developed and more complex (Fig. 2). The sequence ranges upward from lithian biotite granites to muscovite – microcline – albite granites to amazonitic K-feldspar – albite granites with Li–Fe mica and topaz. Typical for Orlovka are pegmatitic quartz – amazonitic K-feldspar bodies near the endocontact. The main accessory minerals in the granites include fluorite, topaz, monazite, xenotime and zircon. The ore minerals are columbite-tantalite, microlite, euxenite and "strüverite". The unit richest

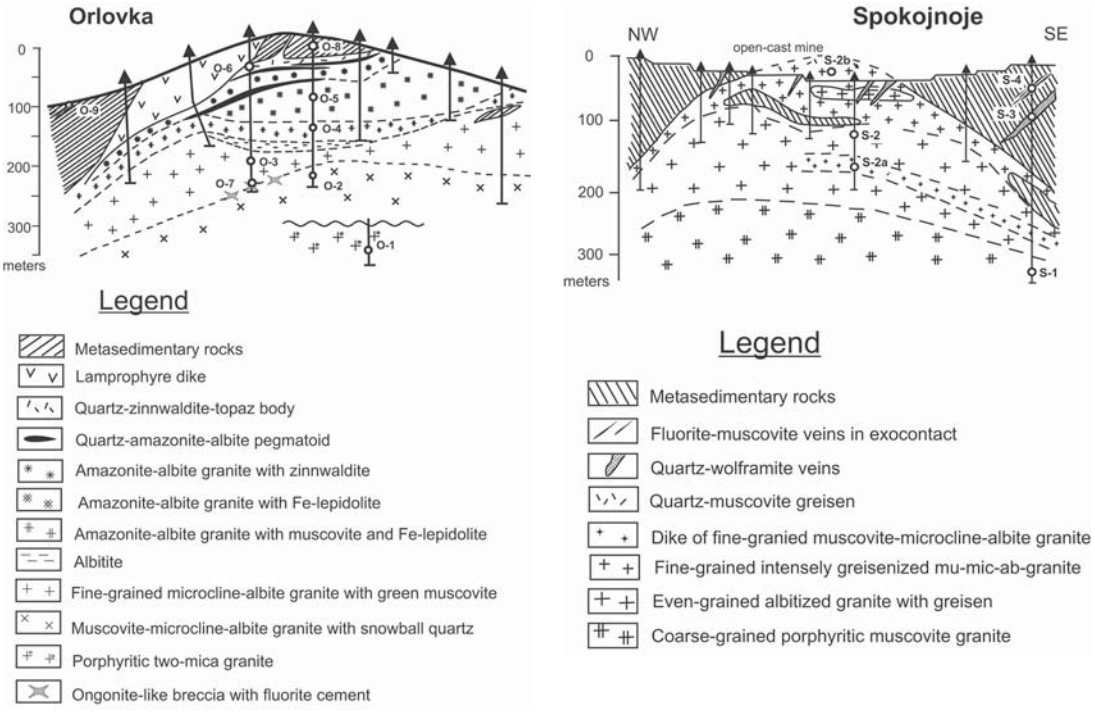

FIG. 2. Interpretative cross-sections through the Orlovka and Spokojnoje intrusions, showing the location of diamond-drill cores and lithologic zones where samples for this study were taken. See Table 1 for description of lithologies. For unit Orlovka O–6, we distinguish pegmatite (O–6–P) and endogreisen (O–6–G).

TABLE 1. DESCRIPTION OF FLUORITE AND HOST ROCKS FROM THE KHANGILAY COMPLEX

Unit	Sample	Main lithology	Petrography of fluorite	Accessory minerals*
		Orlovka		
O-1	229	Porphyritic lithian biotite (protolithionite) granite (±Li-Fe-rich muscovite) (deep horizons)	Anhedral grains of spotty-violet fluorite up to 1 mm	Zircon, apatite, monazite, rutile
O-2	2299	Porphyroblastic m.g. muscovite-microcline-albite granite with snowball quartz	Light brown (reddish) fluorite intergrown with quartz and albite	Zircon, apatite, monazite, xenotime, "strüverite"
O-3	2300	Equigranular, f.g. microcline-albite-muscovite granite with green muscovite	Anhedral grains of spotty-violet fluorite up to 5 mm	Cassiterite, Fe-Mn hydroxides
O-4	253	Amazonitic K-feldspar - albite m.g. granite with Fe-rich lepidolite	Anhedral grains of spotty-violet fluorite <0.5 mm	Topaz, monazite, xenotime, columbite, microlite
O-5	369	Amazonitic K-feldspar - albite granite with lepidolite	No fluorite in O-5 (W flank), interstitial fluorite in O-5 (E flank)	Topaz, monazite, xenotime, tantalite, cassiterite, microlite
O-6-G	O-6-G/1	Zinnwaldite-topaz greisen from endocontact	Core of zoned crystals up to 1 cm size, bright green color	Beryl, topaz, cassiterite
O-6-G	O-6-G/2	Same	Rim zone, violet color	Same
O-7	201	dike-like breccia with fluorite cement near contact 229 and 2299	Bright violet fluorite with chalcedony	-
O-8	5/98	Quartz - fluorite vein in sandstone	Aggregates of euhedral cubic crystals up to 1 cm, bright green	Pyrite, cassiterite
O-9	4733	Quartz - fluorite veins in hornfels	Green fluorite	Beryl
		Spokojnoje		
S-1	2639	Weakly porphyritic muscovite granite with gray muscovite	Light brown (reddish) up to 1 mm	Apatite, zircon, monazite
S-2	2336	Medium-grained microcline - albite granite with gray and green muscovite	Anhedral crystals up to 1 mm, lilac-violet to black in color	Apatite, zircon, garnet, "wolframite"
S-2a	208	Fine-grained dike of microcline - albite granite in S2	No fluorite present	"Wolframite", garnet, apatite
S-2b	2337	Fine-grained intensely greisenized microcline - albite granite with green muscovite of endocontact zone	No fluorite present	"Wolframite", beryl, apatite, garnet, bertrandite, cassiterite
S-3	84/d	Quartz–"wolframite" veins with fluorite, muscovite in greisenized granite	Crystals of grey to dark violet color, up to 0.5 cm across	"Wolframite", apatite, "hungarite"
S-4	2612	Muscovite - fluorite veins in slates from exocontact	Crystals of bright violet color, up to 2 cm	Cassiterite

* Some of these names refer to groups of minerals. Names shown in quotation marks are not IMA-approved.

in fluorite is the muscovite-bearing microcline–albite granite with "snowball" texture quartz (O–2). In contrast to Spokojnoje, fluorite becomes less abundant in the most evolved units of Orlovka, its place being taken by topaz. In the amazonitic K-feldspar granites of unit O–4, fluorite and topaz coexist. The abundance of fluorite and topaz in unit O–5 alternates, so that both minerals occur together in the O–5 granite at the eastern flank of the intrusion but on the western flank, topaz is the only F-bearing phase in this unit. Finally, in the O–6 unit, amazonitic K-feldspar–quartz pegmatite bodies (O–6–P) contain topaz, whereas the endogreisen (O–6–G) contains fluorite. The antithetic relationships between fluorite and topaz in the granites may offer some insight into evolving melt composition, as discussed in more detail below.

The most differentiated granites, especially in the Orlovka intrusion, show a number of features indicating mineral recrystallization and replacement. Mineral replacement in the Orlovka granite involves albitization in the zone of O–3, where fine-grained albite replaces quartz and, to a lesser extent, microcline and $An_{5–9}$ plagioclase. Albitization locally leads to nearly monomineralic vuggy albitite. Farther up in the intrusion, replacement of muscovite by lepidolite is developed, which locally produced a characteristic ocellar structure of mica intergrowths, and tartan-twinned amazonitic microcline in replacement of albite. Topaz and ore minerals accompany the mineral replacement in places. Finally, the exocontact of Orlovka contains important metasomatic zones of greisenization and albitization of the country rocks. These greisen bodies reach up to 10 m in thickness and include distinctive zinnwaldite – topaz – albite assemblages, locally rich in honey-colored beryl.

Sample Descriptions

Fluorite

Samples for fluorite separates were collected from the major internal zones from the Orlovka and Spokojnoje massifs as well as from hydrothermal rocks in the exocontacts. Brief descriptions of the units sampled and of the type of fluorite within them are given in Table 1. The fluorite varies from colorless to dark green, lilac, violet or almost black, and its morphology is also quite variable. In granites of the Orlovka massif, the fluorite generally forms small anhedral grains or grain clusters, the size of which does not exceed 0.5 mm. As a rule, fluorite is associated with clusters of albite (Fig. 3). Fluorite in porphyritic muscovite – microcline – albite granite and amazonite granite from Orlovka is typically colorless or has spotty violet coloration. The abundant fluorite in endocontact greisens of Orlovka is optically zoned, with green interiors and outer zones of violet color (Fig. 3). Fluorite in granites of the Spokojnoje massif is commonly light brown in color, and it becomes lilac to violet in the apical unit of the massif. In the quartz–"wolframite" veins, fluorite forms massive segregations or, more rarely, well-formed crystals. The best-formed crystals, up to 3 cm in size and green-violet in color, are found in vugs and are typical for the layered veins in the exocontact. There are also thin quartz–muscovite veins with bright violet fluorite. In places, fluorite constitutes the entire vein-filling.

Melt inclusions

Melt inclusions occur in quartz phenocrysts (Fig. 3c; Badanina *et al*. 2004). The lack of clear zoning structures of the host crystals makes any correlation of inclusion trapping and growth zoning impossible, but we interpret the inclusions as primary because of their isolated, random occurrence in the quartz and their large size. The size of melt inclusions varies from 20 to about 150 μm, with most between 50 and 100 μm. Abundant trails of secondary fluid inclusions criss-cross the quartz, and some primary-looking fluid inclusions were noted (L + V, in some samples containing birefringent daughter crystals) but not investigated in this study (see Reyf *et al*. 2000). Some of the larger melt-inclusions are associated with tiny, single-phase fluid inclusions (L or V), which may represent trapped fluid that was lost from the melt inclusion by partial decrepitation in nature. In several cases also, microcracks appear to intersect inclusions after homogenization runs, and we speculate that fracturing may have happened on cooling through the quartz α–β transition. Inclusions where these features are obvious were avoided during analysis, and the results of Badanina *et al*. (2004) suggest that inclusion compositions were not significantly affected, as discussed below. About 90 vol.% of the inclusions at room temperature comprises daughter mineral phases, and a deformed liquid or vapor bubble typically is visible (Fig. 3c). Phase proportions are impossible to judge with accuracy at room temperature owing to the abundance of crystallites, but in general, it appears that inclusions from the more evolved units have greater proportions of fluid phases. Badanina *et al*. (2004) studied the crystalline phases in unhomogenized melt-inclusions based on optical properties, morphology and electron-microprobe data, and identified the following minerals: albite, K-feldspar, micas, zircon, columbite, monazite and fluorite. Most of these phases, including fluorite, also occur as solid inclusions in the quartz host. However, solid phases in the melt-inclusion population of a given sample could all be completely remelted by homogenization and quenching runs at 700–750°C, suggesting that they were not accidentally trapped, but are true daughter phases.

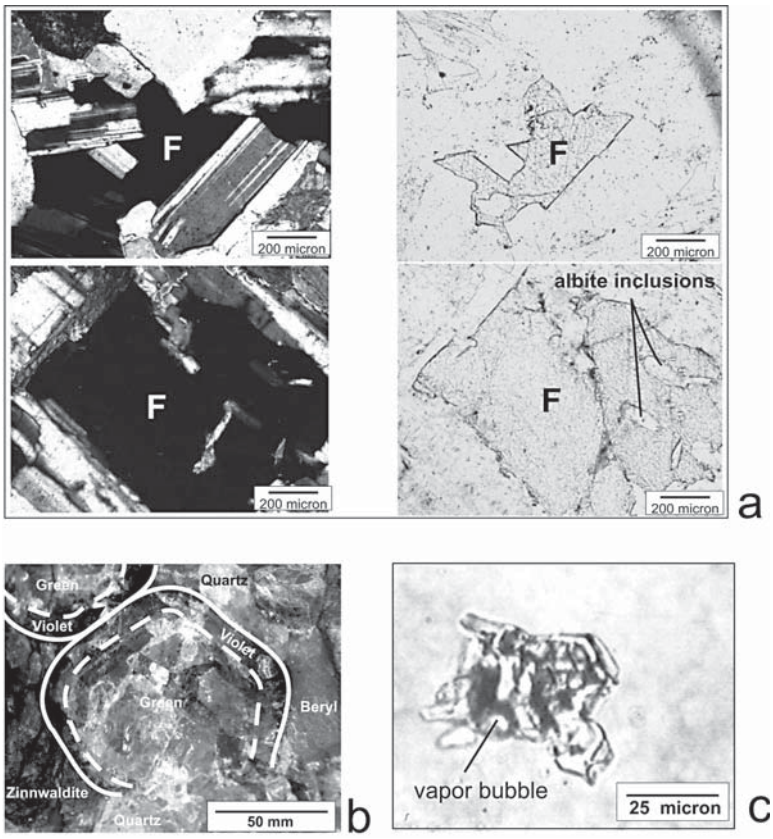

FIG. 3. Photomicrographs showing the typical occurrence of fluorite and melt inclusions in Orlovka and Spokojnoje granites. (a) Accessory fluorite (F) intergrown with albite laths and quartz: top: fluorite with albite in unit O–3; bottom: fluorite–albite intergrowths in unit O–4; note the presence of albite inclusions in fluorite. (b) Zoned crystals of fluorite from zinnwaldite – beryl – quartz zone in Orlovka unit O–6–G (endogreisen). (c) Quartz-hosted melt inclusion from Orlovka granite O–2 at room temperature, showing deformed vapor bubble and aggregates of daughter minerals.

ANALYTICAL METHODS

Bulk-rock and fluorite

Mineral separates of fluorite were prepared from samples of 2 to 6 kg of crushed granite. The granite samples were crushed and sieved to obtain size fractions 0.15–0.2 mm in order to disaggregate fluorite from grain clusters. After magnetic separation, fluorite was extracted from the non-magnetic fraction by heavy-liquid separation (bromoform, Clerici solution) at St. Petersburg State University. Finally, all samples were carefully hand-picked under the binocular microscope. Trace-element analyses of whole-rock granite samples and fluorite separates were performed by inductively coupled plasma – mass spectrometry (ICP–MS) at the GeoForschungsZentrum Potsdam (GFZ) using methods described in detail by Dulski (1994, 2001) and Bau *et al*. (2003). Samples were ground in an agate mortar and about 0.1 g of powder was digested in HF–$HClO_4$ (rock) or HF–HNO_3 (fluorite) under pressure. After dissolution, the solutions were then filled to 50 mL volume with 0.5 N HCl and doped with Ru and Re as internal standards. The ICP–MS measurements were performed with an ELAN 5000A instrument (Perkin–Elmer – SCIEX), and quantification of element concentrations was based on calibration of solutions prepared from external reference samples. Replicate analyses of an in-house fluorite reference solution C5–FL showed a precision for REE and Y of better than 3% (5% for Eu). For lack of secondary reference-samples for REE and Y in fluorite, the accuracy was assessed to be within 10% relative based on a comparison of values from C5–FL obtained by independent analytical techniques (see Bau *et al*. 2003).

Melt inclusions

Our trace-element study was performed on the identical melt-inclusions that were analyzed by electron microprobe for major elements by Badanina *et al*. (2004). Whereas the previous study included melt inclusions from most internal units of the Khangilay, Spokojnoje and Orlovka granites, the scope of our trace-element analyses is limited to the most evolved Orlovka granite, units O–2, O–5 and pegmatite O–6 (P). To minimize decrepitation and leakage, the inclusions were heated in rapid-quench cold-seal pressure vessels at 200 MPa and 700°C to 750°C for 24 hours (procedure described by Badanina *et al*. 2004).

Electron-microprobe analysis of carbon-coated grain mounts employed Cameca SX–50 and SX–100 microprobes at the GFZ. Operating conditions of both instruments were the same, with an accelerating voltage of 15 kV and a beam current of 10 nA. To minimize element migration during electron bombardment, we used a 10 to 40 μm defocused beam, depending on the size of inclusions, and counting times of 20 s for most elements and 40 s for F, P and Rb. Calibration employed synthetic oxides and natural mineral samples, and data reduction used the PAP scheme. Rubidium was calibrated with synthetic rubidine feldspar crystals prepared by S. Melzer, GFZ Potsdam. A full description of analytical conditions for silicate glasses with the SX–100, including estimates of analytical errors, is given in Jochum *et al*. (2000). Analytical accuracy was better than 5% relative for all elements present at abundances >1 wt.%, and 10% for others.

We used the Cameca ims 6f SIMS instrument in Potsdam to analyze the glass from selected, rehomogenized melt-inclusions for both heavy elements (Nb and 14 REE) and light elements (Li, Be and B). Each of the selected inclusions had been analyzed previously for major elements, F and Rb by EPMA, and some for boron (see Badanina *et al*. 2004). Samples were imaged in back-scattered-electron mode prior to analysis to precisely define the inclusion morphology. Unfortunately, it proved impossible to measure Ta by this method because the extraction plate of the SIMS 6f instrument is made of Ta metal.

The two suites of elements require quite distinct analytical conditions, so two analytical series were conducted, between which the sample was cleaned and recoated with a 35-nm film of high-purity conductive gold. For the heavy elements, the instrument was operated with a 20 nA, $^{16}O^-$ primary beam with a nominal 12.5 kV potential, which was focused to a ~30 μm diameter spot on the sample surface. Prior to each analysis, a 3-minute preburn was conducted in order to remove locally the gold film and achieve equilibrium conditions of sputtering. Secondary ions were accelerated through a 10 kV extraction potential. The mass spectrometer was operated at low mass-resolution power, $M/\Delta M \approx 400$, and a 125 V energy offset was applied to a 50 V energy bandpass. Each analysis consisted of 12 cycles of the peak-stepping sequence, which resulted in a total time of analysis of 98 minutes. Secondary ion yields were calibrated against the $^{30}Si^+$ peak, and the NIST SRM610 glass was used as primary reference sample (Pearce *et al*. 1997). Secondary reference-samples were used to evaluate the accuracy of the method and to assess if variations in H_2O contents of individual inclusions affected the relative sensitivity-factors (Wiedenbeck *et al*. 2001). These included a suite of hydrated 610 glass samples (maximum H_2O content 3.87 wt.%), the ATHO synthetic rhyolite (Jochum *et al*. 2000) and the synthetic basalt TB–1G (Potts *et al*. 2002). Analysis of the secondary reference glasses revealed acceptable accuracy for all elements (Appendix).

The concentrations of Li, Be and B were determined on the same inclusions after a light repolish, cleaning and gold coating. An 8 nA, $^{16}O^-$ primary beam, focused to a ~15 μm diameter spot, was used to presputter the locations targeted by previous analyses. For these light elements, the instrument was operated at $M/\Delta M \approx 3000$, which is adequate to eliminate all significant hydride and multiply charged isobaric interferences from this part of the mass spectrum. A 50 V energy bandpass was used, to which no energy filtering was applied. A single analysis, consisting of 12 cycles of the peak-stepping sequence, had a total duration of 9 minutes. The relative sensitivity-factors for each of these three elements were determined using $^{30}Si^+$ using the NIST SRM610 glass (Pearce *et al*. 1997). In some cases, the $^7Li^+$ signal was above the 1.2 MHz threshold of the SIMS digital ion counter, in which case the analysis was rerun with a 400 pA primary beam intensity. For each analysis that was conducted at the lower primary current, the relative sensitivity factors defined by the SRM610 reference sample, run at the lower setting, were employed.

Results

Whole-rock data are reported in Table 2, fluorite data, in Table 3 and melt-inclusion data in Table 4. To achieve a simple and uniform description of REE characteristics in the different samples, we place emphasis on the following features (Fig. 4): 1) the sum of REE concentration (ΣREE), 2) the shape of chondrite-normalized REE patterns and the ratio of light to heavy REE (La/Yb, with values normalized to chondrite abundances from Sun & McDonough 1989), 3) the Eu/Eu* ratio, where Eu* is calculated as $(Sm*Gd)^{0.5}$, and 4) the lanthanide tetrad effect, which describes curved segmented patterns on chondrite-normalized REE diagrams. The segments (tetrads) comprise four elements, and ideally there are four tetrads, but the absence of Pm in nature and the very common presence of a negative Eu anomaly typically disrupts the second tetrad (see Masuda *et al*. 1987, Bau 1996,

TABLE 2. COMPOSITION OF GRANITES FROM THE KHANGILAY COMPLEX, IN TERMS OF MAJOR AND TRACE ELEMENTS

Unit	Kh-1	Kh-2	O-1	O-2	O-4	O-5	S-1	S-2	S-2a	S-2b
Sample	270	422	229	2299	253	369	2639	2336	208	2337
SiO_2 wt%	74.6	75.5	73.0	74.4	72.5	70.3	73.3	73.9	74.3	77.0
TiO_2	0.25	0.24	0.16	0.03	0.01	0.01	0.1	0.1	0.01	0.06
Al_2O_3	13.6	13.7	14.1	13.4	15.6	16.8	14.3	14.1	14.4	12.9
FeO(total)	1.82	0.95	1.65	0.72	0.64	0.58	1.1	1.2	0.77	0.86
MnO	0.04	0.04	0.051	0.05	0.24	0.12	0.1	0.1	0.17	0.09
MgO	0.35	0.35	0.28	0.37	0.1	0.5	0.3	0.3	0.11	0.16
CaO	0.57	0.21	0.89	0.28	0.21	0.14	0.8	0.9	0.29	0.14
Na_2O	3.88	4.53	4.03	4.58	5.61	6.15	4.3	4.0	3.72	4.18
K_2O	5.00	5.38	4.60	4.65	2.69	5.04	5.14	4.73	2.40	4.04
Total	100.1	100.8	98.8	98.5	97.6	99.7	99.3	99.4	96.2	99.4
Li ppm	150	118	395	534	1599	3601	170	129	83	93
F	1600	800	3800	3590	14200	10400	3800	4600	3200	2800
W	5.8	13.2	2.1	3.6	11.3	43	26	88	3200	2500
Rb	726	448	755	1177	1338	3305	418	424	483	610
Sr	73.9	39.7	88.8	16.2	9.02	3.33	90.3	22.9	15.9	12.8
Y	39.4	32.8	34.1	65.6	5.18	2.67	14.9	7.83	10.7	9.56
Zr	109	51.9	99.0	64.3	21.3	42.5	58.4	19.6	23.4	24.0
Nb	36.9	30.6	33.3	67.1	58.8	152	23.5	16.8	53.0	38.4
Cs	39.7	25.8	54.2	46.7	29.9	73.3	35.7	44.1	49.3	62.9
Ba	175	71.6	188	36.9	6.22	4.49	305	26.8	40.2	45.1
Hf	5	2.81	4.61	7.7	4.51	17.8	2.5	1.63	1.58	1.56
Ta	16.5	8.1	14.7	43	69	254	10.4	2.66	4.89	9.89
Pb	57	47	53	66	63	58	46	41	54	32
Th	23.9	15.1	19.9	16.6	9.1	18.1	15	6.1	8.02	8.83
U	10.4	10.3	21.1	8.87	5.49	9.72	25.7	7.75	5.92	11
La	46.4	19.7	23.8	10.5	5.15	2.79	13.4	3.39	5.11	6.3
Ce	66.0	25.6	48.9	27.8	15.0	12.7	28.0	7.53	11.4	14
Pr	7.54	3.05	5.44	3.66	1.76	1.67	3.2	0.91	1.34	1.68
Nd	27	11.4	19.8	15.0	5.05	4.06	11.6	3.36	4.9	6.17
Sm	7.09	3.82	4.88	7.12	2.52	1.74	3.08	1.24	1.68	2.23
Eu	0.36	0.13	0.36	0.06	< 0.03	< 0.03	0.29	0.05	0.07	0.08
Gd	6.77	4.30	5.03	8.51	1.63	0.94	2.89	1.28	1.82	2.08
Tb	1.18	0.88	0.95	1.82	0.47	0.24	0.47	0.28	0.36	0.39
Dy	7.27	5.94	6.04	11.9	2.7	1.39	2.78	1.47	2.08	2.13
Ho	1.21	1.09	1.11	2.16	0.40	0.20	0.46	0.23	0.33	0.318
Er	3.46	3.39	3.19	6.27	1.11	0.54	1.33	0.58	0.92	0.79
Tm	0.52	0.53	0.48	0.95	0.20	0.11	0.18	0.09	0.15	0.12
Yb	2.62	1.86	3.48	6.85	1.51	0.89	1.25	0.67	1.17	0.9
Lu	0.52	0.54	0.46	0.93	0.18	0.11	0.18	0.09	0.16	0.12
ΣREE	165	76	124	104	38	27	69	21	31	37
La/Yb	6.05	2.17	4.90	1.10	2.45	2.25	7.69	3.63	3.13	5.02
Eu/Eu*	0.16	0.10	0.22	0.02	<0.05	<0.07	0.30	0.13	0.13	0.11
t(1)	1.06	1.07	1.05	1.13	1.42	1.92	1.07	1.09	1.09	1.09
t(3)	1.14	1.18	1.13	1.21	1.54	1.47	1.1	1.32	1.25	1.24
t(4)	1.03	1.03	1.05	1.04	1.21	1.28	0.95	1.03	1.08	1.09

Concentrations of the major elements and W were established by XRF (St. Petersburg), F by ion-selective electrodes (St. Petersburg). Those of all other trace elements by ICP-MS (GFZ Potsdam).

Eu/Eu* = $(Sm*Gd)^{0.5}$, La/Yb = ratio of C1 chondrite-normalized values (Sun & McDonough 1989). t(1), t(2), t(3) are values of the lanthanide tetrad effect from Monecke *et al.* (2002).

1997, Irber 1999, Monecke *et al*. 2002). To quantify the tetrad effect, we use the simpler of two schemes in Monecke *et al*. (2002), which yield "t(n)" values where n denotes the first, third, or fourth tetrad. The values are unity for no tetrad effect, greater than one for convex-upward patterns (M shape) and less than one for concave-upward patterns (W shape). Allowing for analytical errors of 10%, the tetrad effect is considered statistically significant for t < 0.8 or t >1.2 (Monecke *et al*. 2002).

Trace elements in whole rocks

The Khangilay granite is the largest and least-differentiated intrusion in the complex; it is not mineralized. The biotite granite (unit Kh–1) yielded the highest whole-rock REE concentrations of all the granites analyzed (ΣREE = 165 ppm), and also the highest La/Yb ratios (12), and a comparatively small negative europium anomaly (Eu/Eu* = 0.16). The overlying muscovite granite (Kh–2) has about half as much total

TABLE 3. TRACE-ELEMENT CONCENTRATIONS IN FLUORITE FROM THE KHANGILAY COMPLEX

Unit	O-1	O-2	O-3	O-4	O-6-G	O-6-G	O-7	O-8	O-9	S-1	S-2	S-3	S-4
Sample	229	2299	2300	253	0-6-G/1	0-6-G/2	201	5/98	4733	2639	2336	84/D	2612
Rb	7.63	**42**	**58**	13.4	0.56	0.64	4.76	0.31		2.81	12.8	0.68	0.88
Sr	53.9	167	139	237	40.4	2231	430	83.6	450	741	348	52.9	947
Y	1045	3375	2062	1577	3456	18.1	21.3	16.5	20.1	698	586	391	185
Zr	**28**	**483**	**150**	**175**	1.1	0.6	0.7	0.43	2.18	**319**	**44**	1.13	0.49
Nb	4.44	**71**	**242**	**68**	0.11	0.06	0.13			7.9	5.4	0.24	0
Cs	0.65	1.64	1.87	0.81	0.39	0.04	0.62	0.07	0.01	0.28	0.75	0.06	0.04
Ba	1.68	1.86	3.3	2.75	1.42	9.81	2.86	7.99	0.64	1.36	**1641**	0.68	0.3
Hf	1.82	**27**	**24**	**55.0**	0.61	0.04	0.06	0.01	0.06	17	1.74	0.05	0.02
Ta	3.96	**32**	**82**	**132**	0.54	0.1	0.1		0.06	3.39	3.06	0.07	0.03
Pb	4.82	**57**	**179**	**47**	1.34	0.24	2.62	0.29	0.93	27.1	3	1.54	0.41
Th	8.29	**50**	**185**	**133**	**65.5**	0.33	0.2	0.1		1.73	5.08	0.04	0.04
U	1.98	**21**	**33**	10	1.13	0.27	0.62	0.24	0.05	7.8	4.76	0.14	
La	18.5	57.9	264	105	109	2.26	0.61	4.47	6.7	10.5	76.4	0.98	0.09
Ce	46.0	148	894	432	493	8.81	1.13	7.75	15.9	25.7	220	4.71	0.52
Pr	7.49	25.2	143	78.2	91.9	1.33	0.2	1.11	2	4.15	33.1	1.29	0.16
Nd	40.6	132	570	299	367	4.38	0.72	4.62	7.29	23.2	147	10.4	1.6
Sm	35.0	157	370	231	384	3.72	0.38	1.36	2.74	14.9	85.5	11.1	2.2
Eu	1.09	1.1	0.28	0.11	0.22	<0.03	0.06	0.4	3.8	3.2	5.99	0.47	1.87
Gd	70.4	306	385	219	439	4.15	0.74	1.81	3.19	31.6	118	23.2	7.33
Tb	20.9	80.8	99.1	69.4	134	1.15	0.23	0.39	0.65	6.44	23.8	2.32	1.97
Dy	133	533	619	390	865	6.94	1.94	2.71	3.72	40.9	114	14.8	14.8
Ho	27.2	94.7	94.8	65.2	129	0.97	0.39	0.56	0.57	7.68	15	2.19	3.1
Er	78.9	286	261	176	367	2.77	1.2	1.69	1.41	21.6	33.9	5.01	9.09
Tm	13.0	46.2	41.5	28.4	62.8	0.45	0.18	0.23	0.2	2.97	4.03	0.58	1.17
Yb	89.1	338	286	185	446	3.32	1.15	1.56	1.42	19.7	22.5	3.49	7.04
Lu	12.7	46.4	34.5	22.3	50.5	0.39	0.14	0.21	0.17	2.69	2.67	0.46	0.88
ΣREE	594	2252	4062	2301	3938	41	9	29	50	215	902	81	52
La/Yb	0.14	0.12	0.64	0.39	0.17	0.47	0.37	1.98	3.27	0.37	2.35	0.19	0.01
Eu/Eu*	0.07	0.02	0.002	0.001	0.002	<0.02	0.34	0.77	3.90	0.45	0.18	0.09	1.41
t(1)	0.95	0.98	1.29	1.45	1.49	1.52	1	0.9	1.13	0.93	1.13	1.08	1.06
t(3)	1.34	1.36	1.44	1.53	1.59	1.57	1.38	1.14	1.28	1.16	1.38	0.91	1.26
t(4)	1.06	1.07	1.13	1.14	1.21	1.16	1.1	0.99	1.07	0.99	0.99	0.93	1.0

The concentrations of trace elements in fluorite mineral separates, reported in ppm, were established by ICP-MS analyses at GFZ Potsdam.
The high values of Rb and HFS elements in some samples (bold type) are unlikely to be intrinsic to the fluorite and probably represent mineral impurities.
Eu/Eu* = $(Sm*Gd)^{0.5}$, La/Yb = ratio of C1 chondrite-normalized values (Sun & McDonough 1989).
t(1), t(2), t(3) are values of the lanthanide tetrad effect from Monecke *et al*. (2002).

TABLE 4. MAJOR AND TRACE ELEMENT CONTENTS OF HOMOGENIZED MELT-INCLUSIONS FROM THE ORLOVKA GRANITE

Unit/zone	O-2	O-2	O-2	O-2	O-5	O-5
Inclusion	230-4A	230-4B	230-4C	230-4D	626-1A	626-4A
pts anal.	2	1	1	2	2	2
SiO_2	70.0 (1.2)	71.6	69.2	69.6 (0.5)	66.4 (0.17)	67.6 (0.57)
TiO_2	0.09(0.05)	0.02	0.04	0.0 (0.0)	0.04(0.01)	0.02(0.00)
Al_2O_3	11.4 (0.41)	11.9	13.2	12.3 (0.71)	12.9 (0.07)	11.6 (0.03)
FeO	0.77(0.25)	0.24	0.16	0.02(0.01)	0.80(0.08)	0.55(0.01)
MnO	0.18(0.04)	0.06	0.09	0.02(0.02)	0.38(0.01)	0.70(0.01)
MgO	0.03(0.03)	0.01	0.03	0.0 (0.0)	0.10(0.01)	0.01(0.01)
CaO	0.08(0.02)	0.13	0.06	0.18(0.02)	0.82(0.04)	0.02(0.02)
Na_2O	2.84(0.12)	2.87	4.44	3.31(0.26)	3.66(0.25)	3.75(0.12)
K_2O	3.20(0.03)	3.38	2.72	3.63(0.11)	1.73(0.05)	2.31(0.01)
P_2O_5	0.03(0.00)	0.01	0.01	0.02(0.03)	0.01(0.01)	0.00(0.00)
Rb_2O	0.32(0.01)	0.32	0.28	0.34(0.04)	0.18(0.01)	0.22(0.00)
F	0.59(0.03)	0.30	0.60	0.20(0.08)	1.59(0.03)	1.71(0.01)
H_2O	[11.4]	[9.8]	[10.0]	[11.0]	7.0	[12.4]
La	0.19 (± 3%)	1.01 (± 3%)	1.25 (± 2%)	1.31 (± 3%)	15.0 (± 1%)	0.18 (± 5%)
Ce	0.39 (± 5%)	1.95 (± 2%)	2.62 (± 1%)	2.84 (± 3%)	55.6 (± 1%)	0.99 (± 3%)
Pr	0.06 (± 3%)	0.3 (± 8%)	0.34 (± 2%)	0.36 (± 3%)	7.8 (± 1%)	0.12 (± 6%)
Nd	0.19 (± 5%)	0.99 (± 7%)	1.24 (± 4%)	1.17 (± 5%)	23.5 (± 1%)	0.34 (± 7%)
Sm	0.20 (± 10%)	0.65 (± 5%)	0.92 (± 6%)	0.59 (± 4%)	11.1 (± 1%)	0.25 (± 15%)
Eu	0.02 (± 13%)	0.03 (± 10%)	0.05 (± 8%)	0.04 (± 11%)	0.02 (± 25%)	0.003 (± 60%)
Gd	0.21 (± 7%)	0.61 (± 5%)	0.96 (± 4%)	0.37 (± 6%)	6.76 (± 1%)	0.18 (± 12%)
Tb	0.09 (± 5%)	0.22 (± 4%)	0.34 (± 4%)	0.11 (± 5%)	2.23 (± 4%)	0.06 (± 9%)
Dy	0.68 (± 7%)	1.44 (± 4%)	1.86 (± 3%)	0.70 (± 5%)	10.68 (± 1%)	0.37 (± 8%)
Ho	0.12 (± 5%)	0.24 (± 4%)	0.34 (± 6%)	0.10 (± 7%)	2.01 (± 19%)	0.05 (± 11%)
Er	0.39 (± 5%)	0.65 (± 6%)	0.81 (± 4%)	0.34 (± 11%)	3.79 (± 9%)	0.16 (± 8%)
Tm	0.07 (± 21%)	0.11 (± 7%)	0.15 (± 5%)	0.06 (± 7%)	0.59 (± 4%)	0.04 (± 23%)
Yb	0.5 (± 7%)	0.76 (± 5%)	1.06 (± 4%)	0.53 (± 6%)	4.18 (± 3%)	0.24 (± 5%)
Lu	0.1 (± 7%)	0.11 (± 5%)	0.15 (± 5%)	0.08 (± 9%)	0.59 (± 3%)	0.04 (± 11%)
ΣREE	3.2	9.1	12.1	8.6	144	3.0
Eu/Eu*	0.31	0.16	0.16	0.28	0.01	0.04
La/Yb_n	0.26	0.92	0.82	1.71	2.49	0.52
t(1)	1.1	1.1	1.1	1.1	1.6	1.9
t(3)	1.7	1.6	1.5	1.6	1.5	1.7
t(4)	0.9	1.1	1.1	1.1	1.0	1.2
Li	2037 (± 1%)	2411 (± 1%)	2397 (± 1%)	1419 (± 1%)	699 (± 1%)	544 (± 2%)
Be	13.1 (± 2%)	8.4 (± 1%)	7.7 (± 1%)	6.7(± 1%)	21 (± 0.5%)	36 (± 0.5%)
B	24 (± 2%)	276 (± 0.5%)	158 (± 1%)	571 (± 0.4%)	46 (± 1%)	20 (± 1%)
Nb	117 (± 2%)	10 (± 2%)	26 (± 2%)	12 (± 5%)	14.4 (± 3%)	23.9 (± 1%)

Unit/zone	O-6-P	O-6-P	O-6-P	O-6-P	O-6-P	O-6-P
Inclusion	443-2B	443-2C	443-2A	443-6A	443-4B	443-4A
pts anal.	3		4	1	1	3
SiO_2	65.4 (0.75)		64.6 (2.67)	68.3	65.3	67.9 (1.06)
TiO_2	0.01(0.01)		0.01(0.01)	0.01	0.00	0.01(0.01)
Al_2O_3	12.3 (0.52)		13.7 (1.07)	11.7	13.6	11.9 (0.25)
FeO	0.79 (0.15)		0.97(0.16)	0.24	0.51	0.78(0.20)
MnO	0.83(0.12)		0.37(0.09)	0.14	0.17	0.27(0.04)
MgO	0.02(0.01)		0.00(0.00)	0.02	0.00	0.01(0.00)
CaO	0.06(0.01)		0.08(0.02)	0.10	0.26	0.09(0.01)
Na_2O	0.83(0.25)		1.23(0.10)	1.21	1.29	1.08(0.06)
K_2O	5.18(0.05)		5.95(0.19)	5.69	5.84	5.16(0.12)
P_2O_5	0.00(0.00)		0.04(0.01)	0.02	0.02	0.01(0.02)
Rb_2O	0.35(0.02)		0.36(0.02)	0.40	0.36	0.36(0.02)
F	1.32(0.08)		1.37(0.19)	0.91	1.06	1.34(0.03)
H_2O	8.40		[11.7]	[12.5]	[13.0]	[11.2]
La	0.09 (± 6%)	0.071 (±18%)	2.56 (± 1%)	0.57 (± 3%)	0.44 (± 3%)	0.15 (± 4%)
Ce	0.26 (± 7%)	0.21 (± 17%)	5.7 (± 1%)	1.46 (±2%)	1.30 (± 2%)	0.40 (± 4%)
Pr	0.03 (± 11%)	0.02 (± 21%)	0.57 (± 2%)	0.18 (± 5%)	0.18 (± 6%)	0.05 (± 6%)
Nd	0.14 (± 31%)	0.09 (± 36%)	1.37 (± 3%)	0.45 (± 9%)	0.54 (± 9%)	0.17 (± 17%)
Sm	0.04 (± 30%)	0.04 (± 25%)	0.50 (± 8%)	0.22 (± 9%)	0.36 (± 7%)	0.09 (± 9%)
Eu	0.01 (± 40%)	0.002 (±67%)	0.02 (± 24%)	0.02 (± 16%)	0.02 (± 23%)	0.01 (± 26%)
Gd	0.05 (± 24%)	0.03 (± 27%)	0.25 (± 9%)	0.21 (± 7%)	0.28 (± 8%)	0.07 (± 10%)
Tb	0.01 (± 14%)	0.01 (±19%)	0.06 (± 12%)	0.08 (± 6%)	0.11 (± 12%)	0.02 (± 13%)
Dy	0.11 (± 36%)	0.03 (± 33%)	0.22 (± 7%)	0.43 (± 6%)	0.64 (± 8%)	0.14 (± 14%)
Ho	0.02 (± 28%)	0.01 (± 22%)	0.03 (± 20%)	0.08 (± 9%)	0.11 (± 9%)	0.02 (± 18%)
Er	0.03 (± 43%)	0.02 (±25%)	0.08 (± 27%)	0.21 (± 10%)	0.25 (± 10%)	0.16 (± 60%)
Tm	0.01 (± 29%)	0.004 (±25%)	0.01 (± 25%)	0.04 (± 10%)	0.06 (± 9%)	0.01 (± 14%)
Yb	0.05 (± 20%)	0.02 (± 26%)	0.08 (± 14%)	0.29 (± 7%)	0.39 (± 5%)	0.09 (± 12%)
Lu	0.016 (± 30%)	0.004 (±39%)	0.01 (± 15%)	0.05 (± 7%)	0.05 (± 7%)	0.01 (± 17%)
ΣREE	0.9	0.6	11.5	4.3	4.7	1.4
Eu/Eu*	0.68	0.18	0.13	0.31	0.14	0.26
La/Yb_n	1.25	2.46	21.9	1.34	0.77	1.13
t(1)	1.1	1.2	1.3	1.4	1.4	1.3
t(3)	1.2	0.9	1.6	1.6	1.7	1.5
t(4)	1.0	1.1	1.2	1.1	1.3	0.7
Li	2254 (± 2%)	501 (± 1%)	5077 (± 1%)	2652 (± 2%)	3741 (± 3%)	83 (± 2%)
Be	14.7 (± 1%)	1.0 (± 3%)	14.1(± 0.4%)	9.9 (± 1%)	5.8 (± 2%)	0.4 (± 1%)
B	13.0 (± 2%)	1.5 (± 4%)	44.6 (± 1%)	2.9 (± 2%)	5.2 (± 3%)	1.5 (± 1%)
Nb	51 (± 0.5%)	0.1 (± 29%)	14.4 (± 7%)	0.8 (± 8%)	0.3 (± 9%)	7 (± 3%)

Concentrations of the major elements, expressed as wt.% oxides (except for F), were established with an electron microprobe. Means given with standard deviation in parentheses where applicable. The amount of H_2O was established by laser Raman spectroscopy or by difference from microprobe totals (square brackets). Concentrations of the trace elements are quoted in ppm; the results, obtained by SIMS, are reported with in-run precision (one standard deviation of the mean, in percent). Eu/Eu* = $(Sm*Gd)^{0.5}$, La/Yb_n = ratio of C1 chondrite-normalized values (Sun & McDonough 1989).
t(1), t(2), t(3) are calculated values expressing the lanthanide tetrads 1, 2 and 3, from Monecke *et al.* (2002).

REE (76 ppm); the main decrease affects the LREE, so that the chondrite-normalized pattern is less steep (La/Yb = 7.4). We attribute this preferential loss of LREE without much change in HREE concentration to crystallization of monazite (see Discussion). There is a concomitant increase in the size of the negative Eu anomaly (Eu/Eu* = 0.10). Visual inspection of the REE patterns from the Khangilay Kh–1 and Kh–2 units reveals signs of the tetrad effect (Fig. 4), but it is not statistically valid according to the criteria of Monecke *et al*. (2002). The Spokojnoje muscovite granite S–1 has low total REE contents, 69 ppm, an inclined chondrite-normalized pattern of distribution (La/Yb = 7.4) and a moderate negative Eu anomaly (Eu/Eu* = 0.30). The more differentiated Spokojnoje units S–2 and S–2a have lower REE contents ($21 < \Sigma REE < 31$), flatter chondrite-normalized patterns ($3 < La/Yb < 3.5$) and a more pronounced negative Eu anomaly (Eu/Eu* = 0.09). The tetrad effect is not statistically significant for the S–1 unit of the massif, but samples from S–2 and S–2a granites show significantly high values for the third and fourth tetrad (Table 2, Fig. 4).

Within the Orlovka intrusion, the lowest and geochemically least-evolved unit (protolithionite granite O–1) has total REE concentrations of 124 ppm, moderately steep chondrite-normalized pattern (La/Yb = 4.7) and a moderately negative Eu anomaly, with Eu/Eu* = 0.22. There is no significant tetrad effect in this granite. With respect to its REE characteristics, the Orlovka basal unit resembles the Kh–1 and S–1 granites. However, all succeeding units in the Orlovka intrusion are quite different. The muscovite – microcline – albite granite (O–2) has lower total REE contents ($\Sigma REE = 103$); the LREE contents decrease and HREE contents increase slightly. This leads to a very flat chondrite-normalized pattern (La/Yb = 1.1) broken only by the extreme negative Eu anomaly (Eu/Eu* = 0.02). Together, these two features give the "gull-wing" REE pattern considered typical of highly fractionated granites (*e.g.*, Syritso 1993). The REE tetrad effect is weakly developed in unit O–2, being statistically significant only for the third tetrad [t(3) = 1.21]. We have no whole-rock REE data for unit O–3 because of the extensive albitization and mineral heterogeneity. The next higher unit, O–4 (Fe-rich lepidolite – amazonitic K-feldspar – albite granite), has much lower total REE (38 ppm) than O–2. Its chondrite-normalized pattern is flat (La/Yb = 2.4), with a strong negative Eu anomaly (Eu is below detection limit). The tetrad effect is also very strong in this granite, with significant values for the first, third and fourth tetrads (Fig. 4). The uppermost magmatic unit O–5 from Orlovka, the lepidolite – amazonitic K-feldspar – albite granite, continues the trend of decreasing total REE contents (27 ppm), and its REE signature resembles that of the O–4 granite in most respects (La/Yb = 2.2, Eu below detection limit, all tetrads well developed).

In summary, toward the top of all three intrusive bodies, the total REE contents decrease, the La/Yb values become lower, the negative Eu anomaly deepens,

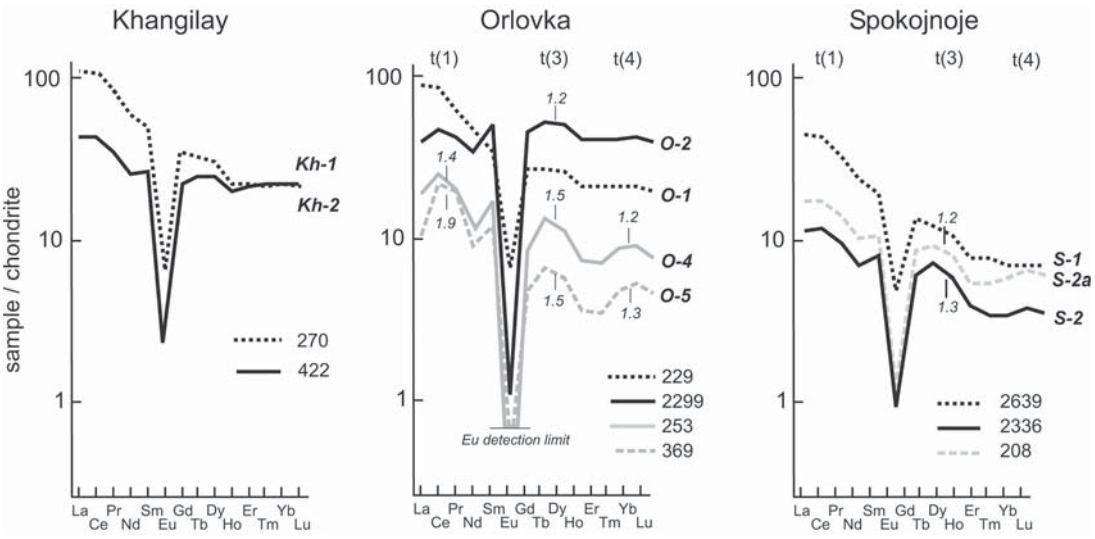

FIG. 4. Chondrite-normalized REE diagrams of whole-rock granite samples from the Khangilay, Spokojnoje and Orlovka intrusions (C1 values from Sun & McDonough 1989). In each diagram, the curves are labeled according to the lithologic unit (O–2, S–1, *etc.*), and sample numbers are given in the legends. Many of the samples, particularly from Orlovka, show the lanthanide tetrad effect (curved, segmented patterns), the magnitude of which is expressed by the t(1), t(3) and t(4) values for the first, third and fourth tetrads, respectively (Monecke *et al*. 2002). Only statistically significant t-values are shown (>1.2).

and the lanthanide tetrad effect becomes prominent. This regularity is shown in selected variation-diagrams (Fig. 5), where we also show trace-element concentrations in fluorite from the corresponding units (as described in the following section). The upper plots on Figure 5 show the magnitude of the t(3) tetrad effect

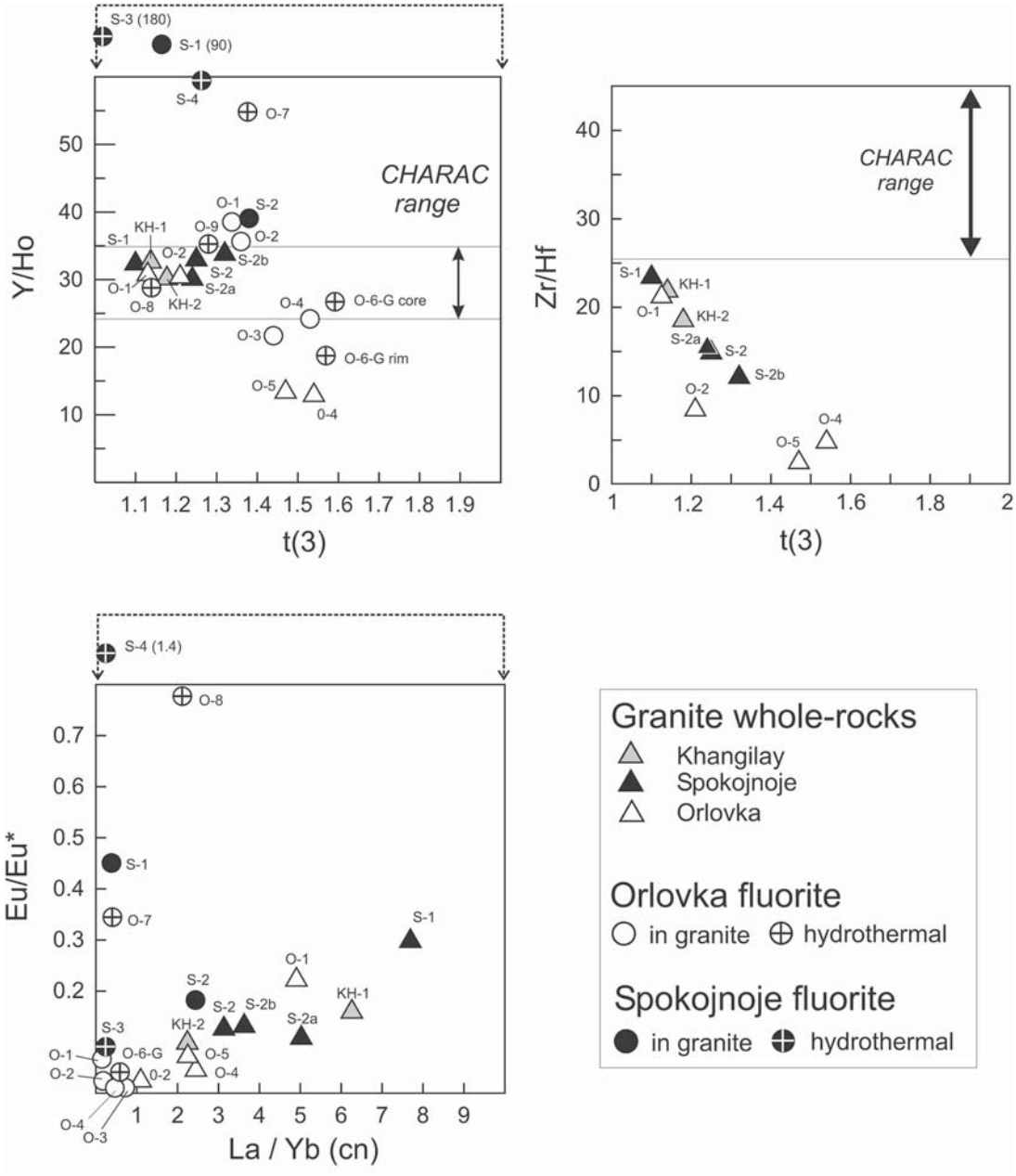

FIG. 5. Whole-rock granite and fluorite samples, showing systematic decrease in Eu/Eu* and La/Yb values (cn: chondrite-normalized), and increase in the tetrad effect [expressed by the t(3) value, see text] with progress of differentiation. The upper panels show variations in Zr/Hf and Y/Ho values relative to the "CHARAC" (charge-radius-control) range proposed by Bau (1996) to discriminate crystal–melt *versus* fluid-phase partitioning. Based on the Y/Ho values, most granite and fluorite samples plot in the CHARAC range; exceptions are the most evolved Orlovka granites O–4 and O–5, and hydrothermal fluorite. All granites show low Zr/Hf values compared with the CHARAC range and show a close correlation with t(3) values.

and Y/Ho or Zr/Hf values. The "CHARAC" (charge-radius-controlled) range was introduced by Bau (1996) to describe the approximate limits of variation of these values that can be expected for melt–crystal partitioning governed by simple electrostatic behavior ("Goldschmidt rules"). Almost all granites from the Khangilay massif (triangles) plot within the CHARAC range for Y/Ho, the exceptions being the uppermost units from Orlovka, O–4 and O–5. In contrast, Zr/Hf values in all granites fall below the range, so for this system, the CHARAC criteria appear not to apply equally to the two element pairs. Linnen & Keppler (2002) showed that subchondritic values of Zr/Hf can result from fractional crystallization in peraluminous granites. A complicating observation, however, is the close linear correlation in the Orlovka granites between Zr/Hf and the tetrad value t(3), shown in Figure 5 (see Discussion).

Trace elements in fluorite

Fluorite concentrates from granites in the Orlovka and Spokojnoje massifs generally have 5–10 times higher total contents of REE than the whole-rock values (Table 3), and in contrast to the granites, the chondrite-normalized REE patterns of fluorite from the lower units O–1 and S–1 have a positive slope, *i.e.*, low La/Yb values (Figs. 6, 7). Toward the top of the massif, the REE patterns of fluorite become flatter and in general, the total concentrations of REE increase. Maximum ΣREE abundances in the Orlovka fluorite are over 4000 ppm (Table 3). The negative Eu anomaly in fluorite hosted by granite (evidence for its magmatic origin is discussed below) becomes more prominent upward in the massif, and the Eu/Eu* values become extreme in the most differentiated units (*e.g.*, 0.07 in O–1 and 0.001 in O–4). All fluorite fractions from Orlovka granites display significant REE tetrad effects, although in the lower units, only the third tetrad has statistical significance. Fluorite from the Spokojnoje granite unit S–1 has no significant tetrad effect, but the third tetrad is well developed in S–2.

Crystals of hydrothermal fluorite from endogreisens in Orlovka (O–6–G) and in Spokojnoje (S–3) show REE patterns that in many ways are similar to their respective magmatic fluorite (compare S–2 and S–3 in Fig. 7, O–4 and O–6–G/1 in Fig. 6). The Orlovka O–6–G fluorite is strongly zoned (Fig. 3), and there is a 100-fold difference in REE contents from core (O–6–G/1)

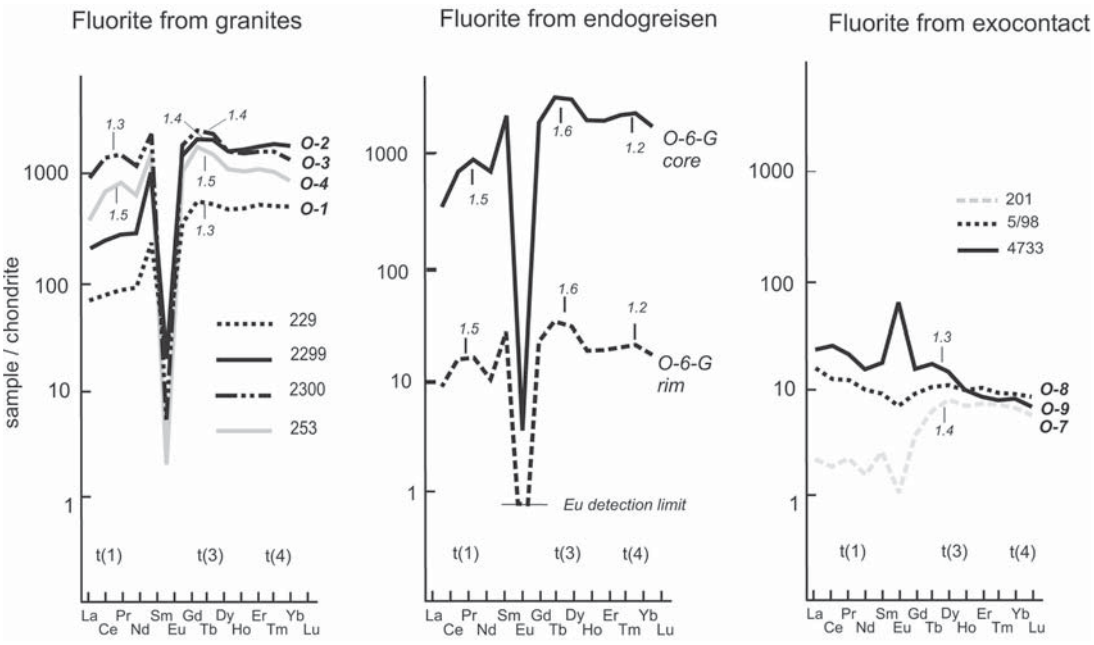

FIG. 6. Chondrite-normalized REE diagrams of fluorite mineral separates from the Orlovka massif. Diagrams are shown separately for fluorite separated from granites, from the zinnwaldite – fluorite – beryl – quartz endogreisen, and from hydrothermal greisen and veins in the exocontact. The curves are labeled according to lithologic unit, and sample numbers are listed in the legends (for O–6–G, unit name and sample number coincide). Hydrothermal units O–7, O–8 and O–9 represent localities at increasing distance from the granite. Important features are the well-developed tetrad effects in late granite units O–3, O–4 [for explanation of t(1), t(3) and t(4) values, see Fig. 4], and the extreme drop in REE abundances between the core and rim of zoned fluorite in endogreisen from zone O–6 (designated O–6–G).

to rim (O–6–G/2), but chondrite-normalized patterns of core and rim are similar in all details, including the strong tetrad effect (Fig. 6). Three fluorite samples from the Orlovka exocontact (O–7, O–8, O–9 in order of increasing distance from the granite) show similar low total abundances of REE, as in the O–6–G rim fluorite (ΣREE <50 ppm), and their chondrite-normalized patterns are highly irregular and bear no resemblance to the patterns for the relevant host-rocks. The same is true for the exocontact fluorite from hydrothermal veins at Spokojnoje (S–4). Figure 5 summarizes some of the important features of the fluorite samples along with corresponding whole-rock data from the granites. Fluorite from unit S–1 has very high Y/Ho and Eu/Eu* values compared to other samples of magmatic fluorite and is similar to many samples of hydrothermal fluorite. We suspect that this difference may be due to inclusion of hydrothermal grains within the fluorite mineral separate from the S–1 granite (see Discussion).

The fluorite separates were analyzed for other trace elements besides the REE, including Y, Sr, Ba, Rb, Zr, Hf, Nb, Ta, Pb, Th and U (Table 3). Some of these elements, like Y and Sr, readily substitute for Ca in the fluorite structure, and are likely to reflect intrinsic values for the fluorite. However, the variable and locally high concentrations of high-field-strength elements like Th, Zr, Hf, Nb, Ta are more likely to result from microscopic inclusions or impurities (as also suggested by Sallet *et al*. 2000). These values are marked in bold type on Table 3 and will not be discussed further.

Trace elements in melt inclusions

Before presenting results on the trace elements, it is useful to summarize the major-element compositional range of melt inclusions and their host granites from the Khangilay massif from Badanina *et al*. (2004). As described in that study, between 3 and 26 inclusions were measured in each sample, and the standard deviations for SiO_2, Al_2O_3, Na_2O and K_2O are 10% of the mean or less. This uniformity of compositions in a given sample and the fact that inclusions plot close to the H_2O-saturated F-rich granite minimum on a normative Qtz–Ab–Or plot suggest that the compositions of the inclusions have not significantly been affected by partial decrepitation or host-mineral fracturing. There may be a problem with overheating and dissolution of host quartz in inclusions from the most evolved units because all homogenization runs used the same temperature and duration, whereas differences in the liquidus temperatures of more- and less-evolved granites can be expected. Artificially high SiO_2 values for inclusions from units S–1, O–5 and O–6 were inferred by Badanina *et al*. (2004) from their position on a Qtz–Ab–Or compared with the other samples. However, overheating is not likely to affect the trace-element concentrations

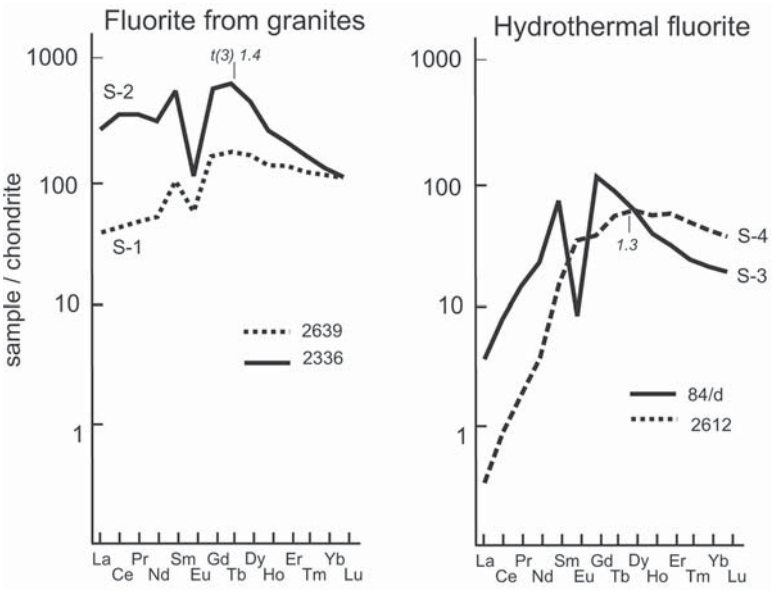

FIG. 7. Chondrite-normalized REE diagrams of fluorite separates from the Spokojnoje massif, shown separately according to the fluorite occurrence in granites and in hydrothermal rocks from the endocontact (S–3) and exocontact quartz veins (S–4). The curves are labeled according to lithologic unit, and sample numbers are listed in the legends.

significantly. All melt inclusions analyzed are peraluminous, with molar A/CNK ratios [Al_2O_3/(CaO + Na_2O + K_2O)] between 1.1 and 1.6. They show trends of increasing F, Rb, Fe/(Fe + Mn), B_2O_3 and decreasing CaO from units Kh–1 to O–5, which mirror the variations in whole-rock composition (Fig. 8). In most cases, the compositions of the inclusions are more differentiated than the respective whole rocks. A critical point emphasized by Badanina *et al*. (2004) is the strong and antithetic shift in alkali element concentrations shown by melt inclusions in pegmatite from unit O–6. This shift was interpreted as reflecting partitioning of alkalis with an exsolved salt-rich hydrous melt.

The melt inclusions have very low REE concentrations: all but one inclusion analyzed yielded total REE values between 1 and 12 ppm (Table 4). A second observation is the large variation in composition of inclusions from single samples. This is very striking in unit O–5, where inclusions 626–1a and 626–4a have ΣREE values of 144 and 3 ppm, respectively, yet similar chondrite-normalized patterns (Fig. 9). Another example is quartz pegmatite sample 443 from O–6–P.

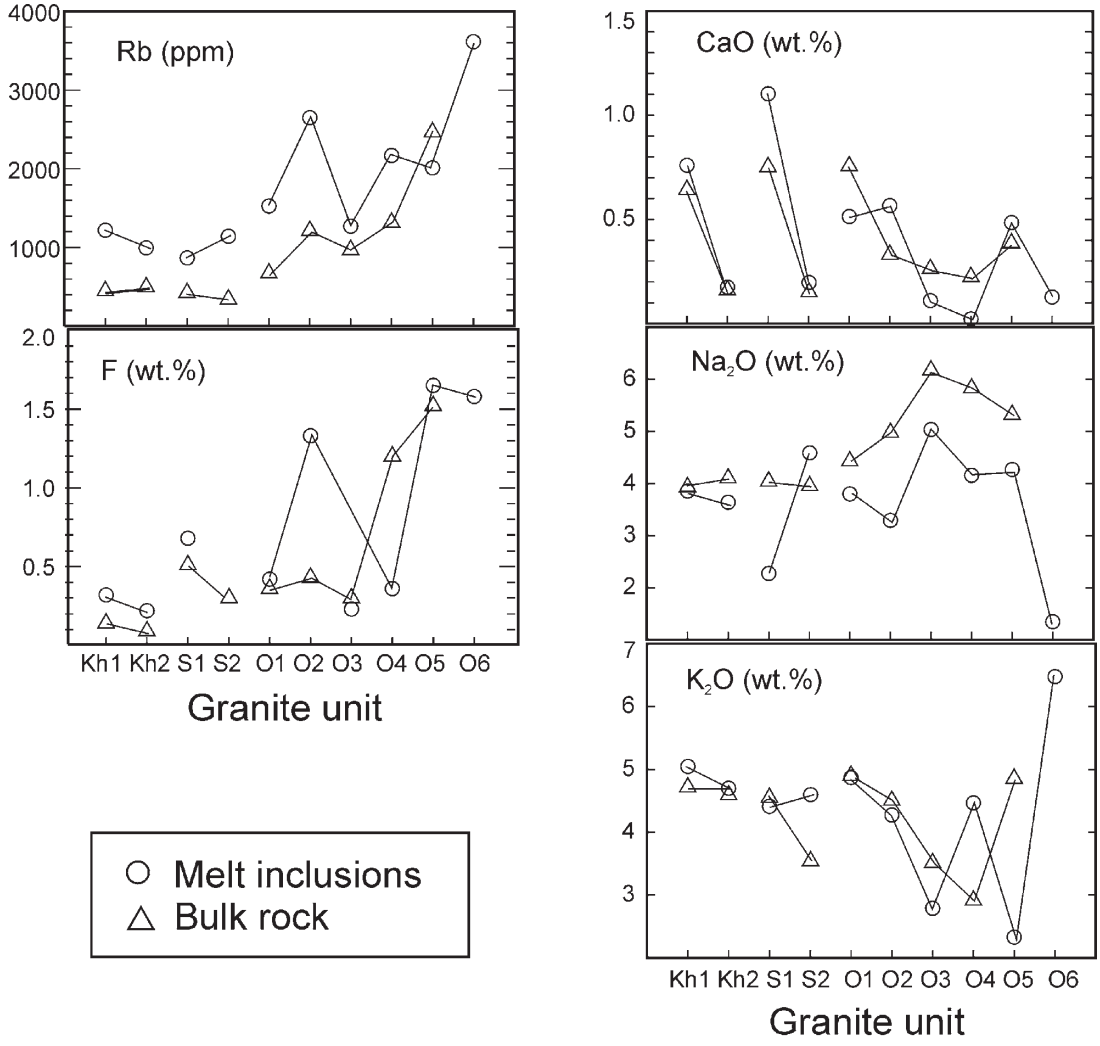

FIG. 8. Average concentrations of major elements, F and Rb in melt inclusions compared with corresponding bulk-rock compositions for the various units of the Khangilay, Spokojnoje and Orlovka granites (see Badanina *et al*. 2004 for data and full descriptions). The sequence of units from left to right corresponds to their relative order of vertical succession in the intrusions. Inclusions from O–6 are in pegmatite quartz, designated O–6–P on Table 4.

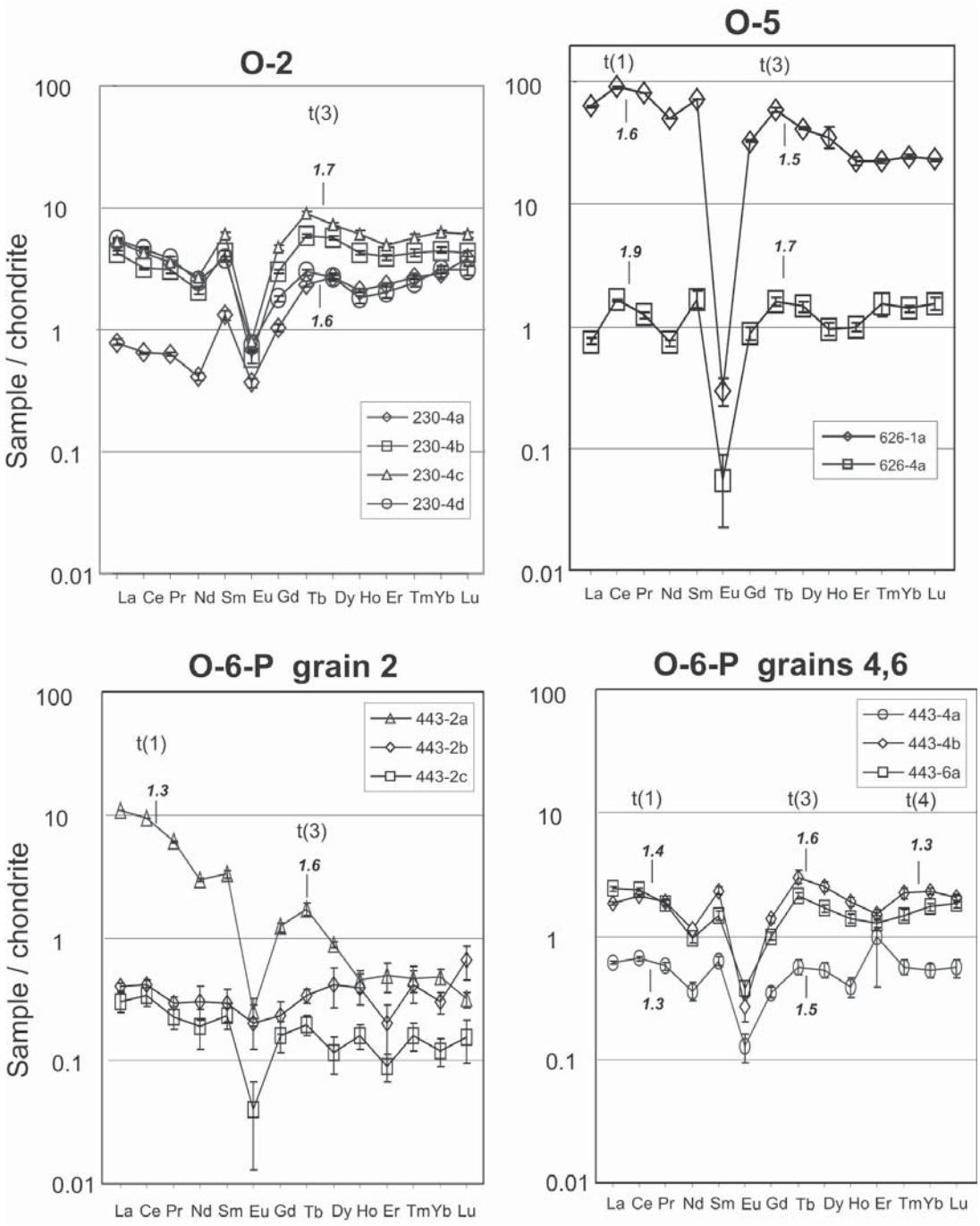

FIG. 9. Chondrite-normalized REE diagrams of homogenized melt-inclusion glasses in quartz from zones O–2, O–5 and O–6 (pegmatite, O–6–P) of the Orlovka intrusion (C1 values from Sun & McDonough 1989). The legends give sample (inclusion) numbers. Error bars represent 1σ (mean) deviation, from Table 4. Note the large diversity of composition of individual inclusions from each zone, and the strong development of the lanthanide tetrad effect in the trapped melts. Only statistically significant values >1.2 are labeled for the t(1), t(3) and t(4) tetrads (see text). REE patterns for the host granites O–2 and O–5 can be compared in Figure 4.

The results from this sample are shown separately for three quartz grains that host the inclusions. In grain 2 (443–2a, –2b, –2c), one inclusion (443–2a) has a comparatively "undifferentiated" REE character, with 11.5 ppm total REE and La/Yb = 22, whereas the other two have less than 1 ppm ΣREE and flat patterns. The three melt inclusions from grains 4 and 6 all have flat REE patterns with prominent negative Eu anomalies, and low but variable ΣREE abundances. Likewise, three of the four inclusions from unit O–2 (sample 230) have nearly identical REE patterns and abundances, and the other has a similar pattern but lower LREE (Fig. 9). In general, the REE patterns of melt inclusions are flat, with a prominent negative Eu anomaly like the host granites. With one exception, normalized La/Yb values are between 0.5 and 2.5, as is also the case for the corresponding whole-rocks (1.1 to 2.4, Table 2). The lanthanide tetrad effect is well developed in the melt inclusions. This is a key finding because it confirms that the tetrad effect is a feature of the melt phase in the Orlovka system and that it cannot have resulted from postmagmatic processes (see Discussion).

One might suppose that the extreme variations and very low REE contents in melt inclusions from sample O–443, grain 2, are the result of the ion beam not being completely within inclusion glass or that it passed into the host quartz during analysis. Examination of the beam craters after analysis, however, shows that they were clearly contained within the inclusions, and "burning through" the inclusions can be ruled out because no systematic drops in concentration were noted during the course of the 12 cycles comprising each analysis. Thus the variations in melt-inclusion compositions appear to reflect real changes in the composition of residual melts, which show a dramatic depletion in REE. One point to emphasize, however, is that the analytical precision for inclusions with less than 1 ppm ΣREE is poor, with errors of more than 25% for several elements at the 1σ level (Table 4).

Our new data for Nb, B, Be and Li compositions in the melt inclusions show large variations within and between samples, and no apparent systematic trends in concentration of melts in the sequence of differentiation O–2 to O–5 (Table 4). Values for Nb are particularly variable, the highest value is 117 ppm for O–2, and there is no trend in Nb with vertical position in the intrusion. The most significant features of the light element contents of melt inclusions are the generally high Li contents, with most samples above 1000 ppm and the maximum of 5100 ppm being found in unit O–6. Lithium shows a weak positive correlation with F in the inclusions (Fig. 10). Boron and Be contents are low (1–36 ppm Be, 1–570 ppm B). The maximum B values correspond to about 0.2 wt.% B_2O_3. The SIMS results for B are consistently lower than values determined by electron-microprobe analysis on the same inclusions (0.3 to 0.9 wt.%, maximum 1.5 wt.%, Table 4). The reason for this discrepancy is not yet known; there does not seem to be any analytical problem with either technique.

Discussion

In the following section, we focus on the distinction between the effects of fractional crystallization in the evolution of the Khangilay granitic magmas and the separation and partitioning of a fluid or a second melt phase. We emphasize the REE and Y results because of features (tetrad effect, Y/Ho fractionation) that may indicate melt–fluid unmixing, and because many of the other trace elements in fluorite likely reflect contamination by mineral impurities. An interpretation of the HFSE and Rb, Cs contents in the whole-rock samples is not warranted because most of these elements have been treated in detail in the geochemical study of Syritso *et al*. (2001), and our analytical results agree well with those already published. We begin by assessing how much of the observed variations in the granite and fluorite samples can be attributed to fractional crystallization and expected mineral–melt partitioning. Then, we point out features in the data for which other processes must be invoked, and discuss whether these can reasonably be attributed to unmixing of an alkali–fluoride hypersaline fluid.

Evidence in favor of magmatic fluorite

The interpretation of the trace-element contents of fluorite separates from the Spokojnoje and Orlovka granites depends on the assumption that this fluorite is magmatic in origin. This aspect needs to be critically assessed. Evidence that some fluorite crystallized from a melt comes from the presence of isolated grains of fluorite included in quartz phenocrysts, which was observed in our study and also noted by Reyf *et al*. (2000). Macroscopic fluorite is commonly an interstitial, late-stage phase intergrown with sodic plagioclase. Local inclusions of albite within fluorite grains indicate contemporary crystallization of the two phases (Fig. 3). Another argument for a magmatic origin of fluorite is the antithetic relationship observed between fluorite and topaz abundance in various units of the Orlovka granites, suggesting an internal control on the relative stability of the two phases. Fluorite is the only mineral of fluorine in units O–1 through O–3 and in Spokojnoje S–1 and S–2. In unit O–4, fluorite and topaz coexist, but fluorite is subordinate, and in unit O–5, the youngest igneous unit in the intrusion, the F-bearing phase is exclusively topaz. The stability of fluorite *versus* topaz is unlikely to be controlled by Ca activity alone, as even in units O–2 and O–3 at Orlovka, Ca levels are extremely low, and they do not appear to drop further in topaz-bearing O–4 and O–5 (Table 2, Fig. 8). Dolejš & Baker (2004) showed that the change from fluorite to topaz stability can reflect a low alkali:aluminum ratio in the melt. This seems a more likely explanation for

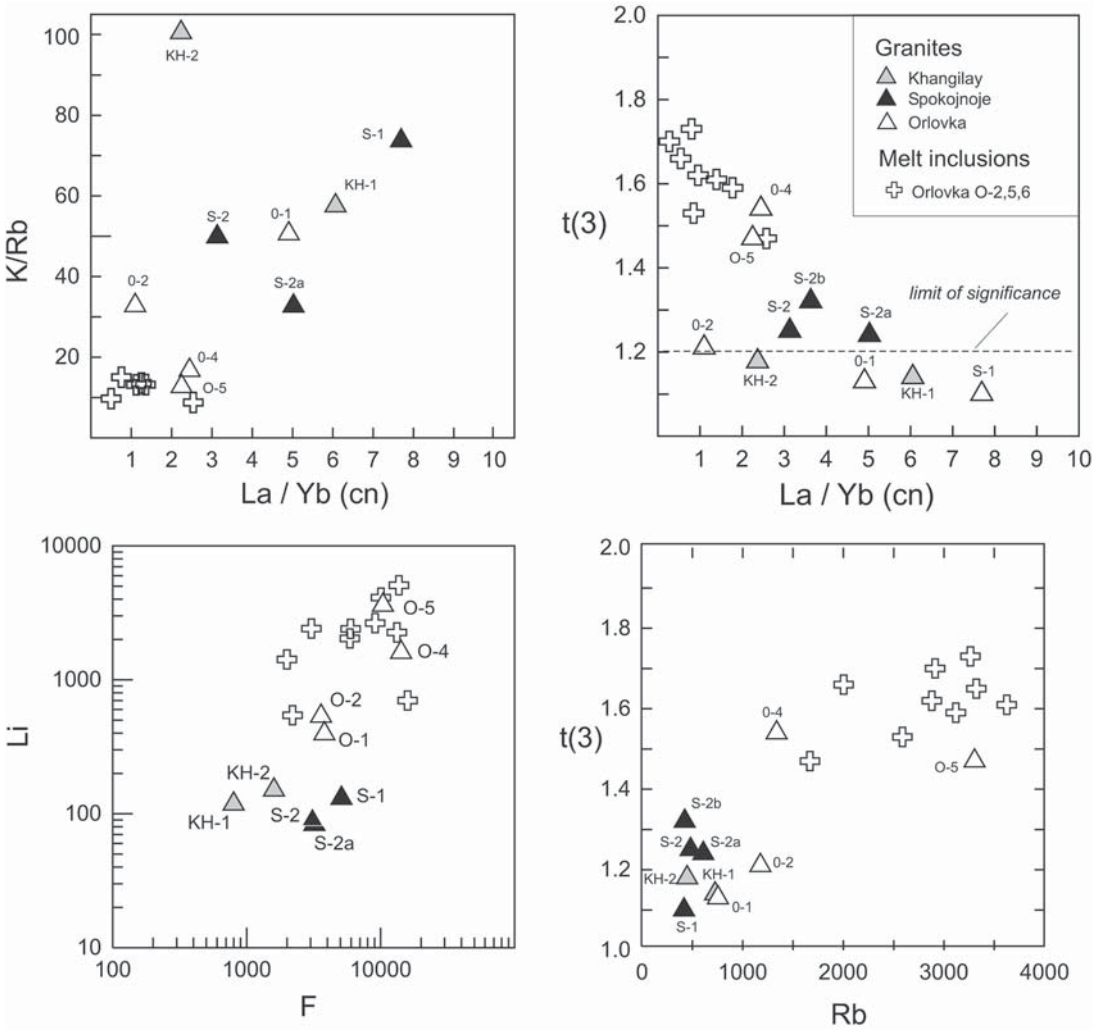

FIG. 10. Comparison of whole-rock fractionation-related trends established from the Khangilay granites with melt-inclusion glasses from Orlovka units O–2, O–5 and O–6 (pegmatite). The inclusions from Orlovka are shown with one symbol because they overlap completely across the different units. Inclusion glasses are more differentiated than the granites and tend to plot along the variation trend defined by whole-rock samples.

Orlovka, where late units do show strong variations in alkali : aluminum ratios (Badanina *et al*. 2004). Finally, the patterns of REE abundance in fluorite from granitic rocks, compared with corresponding melt-inclusion data, are consistent with crystal–melt partitioning data obtained experimentally (Veksler *et al*. 2005) and inferred from fluorite–matrix compositions in rhyolite (Marshall *et al*. 1998), shown in Figure 11. We did not analyze melt inclusions from the Spokojnoje granite for trace elements, but comparison of REE abundances in S–2 fluorite with the composition of aplitic S–2b granite dike yields a rough estimate of fluorite–melt partitioning that also resembles the experimental and empirical curves (Fig. 11). It must be emphasized, however, that the strong REE variations in individual inclusions, coupled with the fact that the fluorite data represent bulk-mineral separates, mean that our results are not suitable for estimating quantitative partition-coefficients for the REE.

Magma evolution I: the effects of crystallization

Regularities in the composition of feldspars, micas and whole-rock samples with the sequence of internal units in the Khangilay, Spokojnoje and Orlovka intrusions suggest that differentiation by fractional crystallization played a dominant role in the evolution of the magmas (Fig. 8). These features were documented by previous authors, and Syritso *et al*. (2001) presented a mass-balance assessment of whole-rock and mineral data which demonstrated that much of the chemical variation in the granites can be accounted for by fractional crystallization. They also found, however, that modeled bulk-partition coefficients for several elements (Zr, Na, K, Be, Sr) abruptly changed in the upper zones of the Orlovka granite (above the snowball quartz layer O–2). The changes were attributed to partitioning with an additional phase, either a volatile-rich melt or an aqueous hydrothermal fluid. We believe that the REE data also indicate fluid–melt partitioning in the more evolved units (see below).

The basal units of the Orlovka, Spokojnoje and Khangilay granites (O–1, S–1 and Kh–1) have very similar REE distribution patterns, supporting other chemical and isotopic arguments for a common parental magma (Syritso *et al*. 2001, Badanina *et al*. 2004). The variations in REE distribution from the basal units to more evolved levels in the three intrusions involve a drop in total REE concentrations, a decrease in La/Yb ratio, a deepening of the negative Eu anomaly, and the development of the tetrad effect. The observed minerals that contain high levels of REE in the granites are accessory fluorite and the phosphates apatite, monazite and xenotime (Table 1). The modal abundances of these accessory minerals are not known, and are likely to vary considerably in the layered granites, so we make no attempt to quantify the effects of their crystallization. Nevertheless, the preferential depletion of the LREE in early stages of magma evolution (*i.e*., Kh–1 to Kh–2, S–1 to S–2, O–1 to O–2 can be attributed to crystallization of a monazite-group mineral, which is present throughout the lower units in the Khangilay complex and is the only REE-rich mineral present with a high La:Yb ratio. The increasing negative Eu anomalies at this stage may be explained by feldspar fractionation. In both the Orlovka and Spokojnoje intrusions, units O–2 and S–2 show development of the tetrad effect. It has been amply demonstrated by Bau (1997) and Irber (1999) that no combination of REE phosphates or other common phases in peraluminous granites can produce a tetrad effect in residual melt. Crystallization of fluorite was not considered by them, but it can easily be ruled out for Orlovka because none of the fluorite shows the complementary W-shaped tetrads that would be required. Thus, already in units S–2 and O–2, the rocks show evidence of a process other than crystal fractionation affecting the REE distribution, and the tetrad effect increases in intensity in all subsequent

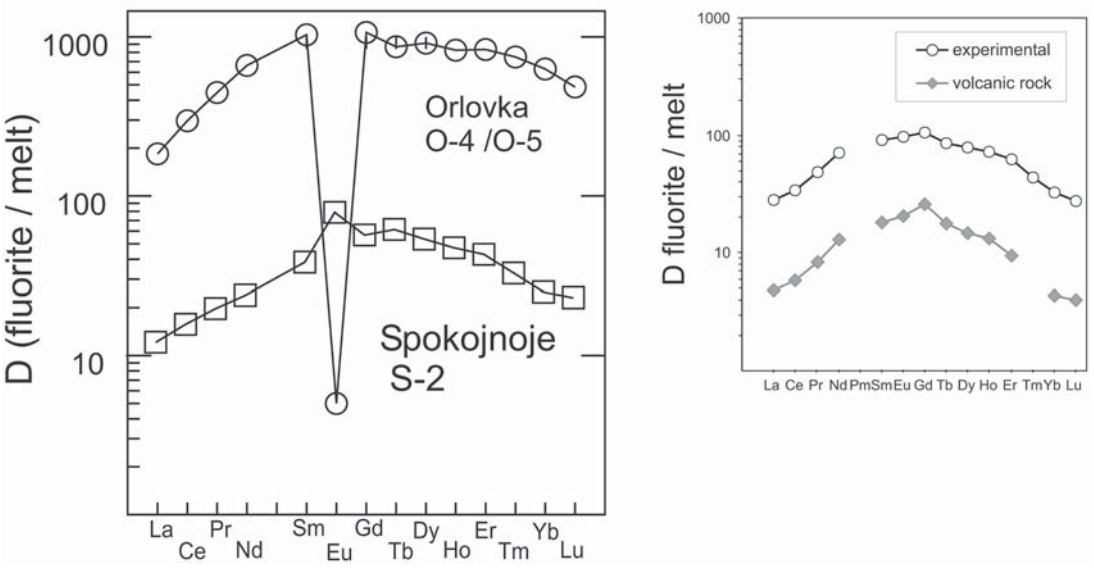

FIG. 11. Fluorite–melt partition coefficients (D values) for the REE based on analytical data on fluorite and quartz-hosted melt inclusions for Orlovka, and on analytical data on fluorite and fine-grained granite dikes for Spokojnoje (see text). The upper diagram shows good agreement between our results and experimentally determined partition-coefficient values by Veksler *et al*. (2005), and empirical values of D from fluorite phenocryst – matrix rhyolite data from Marshall *et al*. (1998).

units of the Orlovka granites. Whole-rock analyses were not carried out for O–3 because of its metasomatic overprint, so the next granite represented by our data is O–4, which has lower total REE contents than O–2 and a negative slope of the chondrite-normalized pattern (Fig. 4). Unit O–5 has an even lower total REE than O–4, but the difference is mostly due to loss of HREE (Fig. 4). In principle, the preferential removal of HREE from O–4 to O–5 could reflect crystallization of a xenotime-group phase, which is present in O–4. Other REE-rich accessory minerals, including fluorite from O–4, lack the necessary high Yb:La ratio. On the other hand, fluid–melt partitioning could also cause preferential removal of HREE (Salvi *et al*. 2000), and a separate fluid phase is likely to have been present in these late, upper units of Orlovka (see below). A potential aid in distinguishing crystal–melt from fluid–melt effects on element behavior in evolved granites is to compare the ratio of elements with similar charge and radius (*e.g*., Y/Ho and Zr/Hf) with the empirically defined "CHARAC-controlled" range from Bau (1996). Except for the most highly evolved O–4 and O–5 units, all samples of Orlovka granite have a Y/Ho ratio in the CHARAC range (Fig. 5). Our interpretation would be that variations in the middle REE are consistent with control by crystallization. On the other hand, all of the samples of Khangilay granite, not just the upper units at Orlovka, have Zr/Hf values below the "CHARAC" range. At face value, this argues for fluid–melt effects, which would contradict the Y/Ho interpretation. Clearly, the issue is more complex, and the "CHARAC test" must be interpreted with caution. Linnen & Keppler (2002) showed that variations in Zr/Hf value in granites depend on melt composition (and structure). They found bulk D_{Hf}/D_{Zr} values near one for peralkaline systems, but less than one for peraluminous granites, and predicted a drop in Zr/Hf with crystallization. This could be the case for the Orlovka granite. However, the close covariations of Zr/Hf and the value t(3) of the REE tetrad effect shown in Figure 5 are inconsistent with fractional crystallization alone (see below).

Most features of the REE compositions of fluorite in the granites conform to the trends of whole-rock variation (compare Figs. 4 and 6), suggesting that fluorite crystallized from evolving magmas with a systematic partitioning of the REE, as described in Figure 11. For example, the whole-rock sequence from O–1 to O–2 shows a decrease in LREE, a flattening of the chondrite-normalized pattern, a deepening of the Eu anomaly, and a slight development of the tetrad effect. The corresponding samples of fluorite show the same relative changes (Fig. 6). The further depletion in REE from O–2 to O–4 in whole rocks is also mirrored in the corresponding samples of fluorite. The fluorite in the Spokojnoje suite, on the other hand, shows a different relationship to the whole-rock REE trends. The granite evolution S–1 to S–2 involves a drop in REE abundance, a flatter chondrite-normalized pattern, a deeper Eu anomaly, and the first appearance of a tetrad effect. Fluorite samples from units S–1 to S–2 also show a deeper Eu anomaly and a tetrad effect (Fig. 7) but in contrast to the granites, REE abundances in S–2 are higher than in S–1, particularly the LREE. The empirical fluorite–melt partitioning for unit S–2 at Spokojnoje appears to be normal (Fig. 11), so an explanation for the lower contents in S–1 fluorite is that the mineral separates from that unit include some hydrothermal grains. Hydrothermal fluorite in the Spokojnoje suite (see below and Fig. 7) has much lower REE than fluorite in the granitic rocks, and particularly strong LREE depletions. Also, the Y/Ho values of fluorite from the Orlovka and Spokojnoje sequences generally plot within the "CHARAC" range, along with corresponding whole-rocks (Fig. 5), but compositions of the S–1 fluorite has much higher values, similar to hydrothermal fluorite in units S–3 and S–4.

Magma evolution II: liquid immiscibility

Previous investigators (Reyf *et al*. 2000, Syritso *et al*. 2001, Badanina *et al*. 2004) have pointed out a number of anomalous features of the Orlovka whole-rock and melt inclusions that are not consistent with simple models of fractional crystallization, and to these can be added the lanthanide tetrad effect and non-CHARAC Y/Ho values revealed in our trace-element study. Similar REE features have been noted in other rare-metal Li–F granites as well (*e.g*., Bau 1996, Helba *et al*. 1997, Irber 1999, Zhao *et al*. 2002). The anomalies are especially vivid in the upper parts of the Orlovka intrusion, starting with the muscovite – microcline – albite granite with "snowball" quartz (unit O–2, Fig. 1). The poikilitic snowball quartz (which features concentric arrangement of albite inclusions) is itself a characteristic and somewhat controversial feature of rare-metal granites, being ascribed by some to metasomatism, and by others to coprecipitation of quartz and albite from a melt (*e.g*., Beus 1982, Schwartz 1992, Yin *et al*. 1995, Helba *et al*. 1997, Müller & Seltmann 1999). A cathodoluminescence study by Müller & Seltmann (1999) revealed complex rhythmic zoning in snowball quartz, which led them to suggest pulses of fluid exsolution, which triggered quartz supersaturation and a rapid increase in its growth rate, trapping albite and other inclusions on growth fronts to produce the snowball texture. Above this zone, the O–3 layer is the first occurrence in the granite of pegmatitic lenses and of locally intense albitization (Fig. 1), the presence of which also suggests important changes in the physical–chemical state of magma, probably related to fluid oversaturation. We have not analyzed whole rocks from unit O–3 for trace elements, but fluorite separates from this unit show extreme tetrad effects, and these continue to be prominent in the later units (Fig. 6), with the strongest development in units O–4 and O–5, which also show non-CHARAC values of the ratio Y/Ho (Fig. 5).

There are two critical observations from our study related to the tetrad effect: (1) it is well-developed in granitic melt inclusions from Orlovka (Fig. 9), so any process invoked to explain the tetrad effect must have affected the Orlovka magma while quartz was still crystallizing, and (2) none of the hydrothermal fluorite in greisen bodies or veins associated with the Khangilay granites show complementary W-shaped tetrads. Fluorine-bearing hydrothermal fluids have commonly been proposed as possible agents for generating the tetrad effect (*e.g.*, Irber 1999, Zhao *et al.* 2002), but little has been specified about the origin and properties of these fluids or the timing of their separation with respect to magma evolution. Fluoride complexes in aqueous fluids can be effective carriers of REE, whether or not the fluids are magmatic in origin (Wood 1990, Salvi & Williams-Jones 1996, Salvi *et al.* 2000), but none of the previous fluid–melt partitioning studies showed signs for a W-shaped tetrad development that could explain the anomalies observed in Orlovka and other granites of its kind. Important progress toward a solution to this problem comes from recent experimental studies showing that hydrous granitic melts enriched in halogens and Li can reach a state of liquid immiscibility above the solidus where silicate melt and a dense, highly saline fluid (hydrosaline melt) can coexist (Veksler *et al.* 2002, Veksler 2004, Webster 2004). As described in the recent review by Veksler (2004), hydrosaline melt can be defined as concentrated, predominantly ionic, dissociated liquid which contain variable, but subordinate amounts of dissolved molecular components, such as H_2O and CO_2. This medium is distinct from and generally immiscible with dilute, predominantly molecular fluids as well as polymerized silicate melts. Its high degree of mobility and strong affinity for HFSE and REE elements (see below) make hydrosaline melt a potent agent for REE transport in late-stage granitic magmas. In most granites, the first hydrosaline melts exsolved are expected to be dominated by chloride species (Roedder 1992, Audétat *et al.* 2000, Webster 2004), but in highly evolved Li–F granites like Orlovka, the hydrosaline melts are likely to become enriched in fluoride components, and should therefore be a major sink for REE and HFSE elements. Experimental studies in synthetic salt–silicate systems by Veksler *et al.* (2005) showed that the fluoride-dominated hydrosaline melts are very effective in concentrating REE generally, and can also produce the selective enrichments that lead to tetrad effects and to separation of Y and Ho. For example, the two-liquid (fluoride/silicate melt) Nernst partition coefficients (D) for the REE in general are 100–200, D_{La}/D_{Lu} are between 2 and 6, D_Y/D_{Ho} is about 1.5, and the first and the last elements of the REE tetrads have slightly but significantly higher D values than their neighbors, giving W-tetrad patterns. Ongoing partitioning studies (Veksler, unpubl. data) show that the F-rich hydrosaline melt also preferentially concentrates Li, Be, and Zr relative to the silicate melt (D_{Li} *ca.* 16) and can effectively separate Zr from Hf or Nb from Ta, with D_{Nb}/D_{Ta} up to 4. Chloride-dominated hydrosaline melts have a lower capacity for extracting REE from silicate magmas and show no sign of developing the lanthanide tetrad effect (Veksler *et al.* 2005).

Thus, it appears that separation of an immiscible F-bearing hydrosaline melt from granitic magma above its solidus may leave the residual silicate melt depleted in Na/K and Li, with very low contents of all REE, subchondritic Y/Ho and Zr/Hf values, and with an M-shaped tetrad pattern, especially prominent in the first and the third tetrads. These features are in qualitative agreement with observed REE patterns in evolved Orlovka rocks, fluorite and melt inclusions. Still unexplained in the case of Orlovka is the geological "fate" of the hydrosaline melt; no inclusions of that phase were found so far (compare Thomas *et al.* 2005), and fluorite from greisen that might be expected to crystallize from such a F-enriched hydrosaline melt have M-shaped tetrad patterns like the granite.

Hydrothermal fluorite and the geochemical "memory"

Fluorite of clearly postmagmatic origin was sampled in endo- and exocontacts of the Orlovka and Spokojnoje intrusions in order to monitor the behavior of REE beyond the magmatic stage of evolution. As discussed above, none of the samples show REE characteristics expected of the hypothetical immiscible hydrosaline melt. The samples of hydrothermal fluorite analyzed so far are characterized by low overall REE concentrations compared to the fluorite from granites, and they were likely deposited from dilute hydrothermal fluids. The contrast between granitic and hydrothermal fluorite is vividly shown by the core and rim compositions of fluorite from the Orlovka endocontact greisen O–6–G (Figs. 3, 6). The inner and outer zones of this fluorite differ in concentrations of some trace elements by two orders of magnitude. The core of this crystal has REE contents close to 4000 ppm, Y about 3460 ppm and chondrite-normalized REE pattern almost identical to fluorite from granitic unit O–4 (Fig. 6). The outer zone is poor in REE (ΣREE 41 ppm) and Y (18 ppm), with concentrations (not patterns) similar to the exocontact fluorite O–8 and O–9 (Table 3). Such abrupt changes in compositions on a millimeter scale argue for crystallization from distinct media; we believe that these zoned crystals of fluorite record the local magmatic–hydrothermal transition at this position in the Orlovka massif. An interesting feature revealed by the zoned crystals from the endogreisens in both Orlovka and Spokojnoje (O–6–G and S–3) is the "chemical memory" of the granite, which has been demonstrated in many other studies and is the basis for using fluorite to trace the origin of mineralizing fluids. Samples of hydrothermal fluorite from Orlovka and Spokojnoje exocontact zones taken at greater distance from the

granites (*e.g.*, O–7, O–8, O–9 and S–3, S–4) appear to reflect increasing interaction of fluid with the country rocks, until ultimately the resemblance to magmatic patterns is lost (Figs. 6, 7).

Conclusions

The Khangilay complex presents a well-documented sequence of differentiation in a granitic system that culminates in highly evolved Li–F leucogranites and economically exploited deposits of Ta and W. Our study is the first to look in detail at the behavior of the rare-earth elements in this system, and the results provide insights into the processes of element enrichment and magma evolution that are likely to be of relevance for rare-metal granites in general.

Accessory fluorite in the granites was shown to be a magmatic phase, on the basis of its mutual crystallization with albite, its presence as inclusions in magmatic quartz, and the correspondence of calculated fluorite–melt distribution-coefficients of the REE with published results from volcanic rocks and from partitioning experiments. Fluorite in the granites responds to changing REE (Y) concentrations in the melt, and we can combine fluorite data with bulk compositions of the host granites and with data on REE in trapped melt-inclusions to reconstruct the behavior of REE during nearly the full range of magma evolution. Fluorite is also abundant in greisen and vein deposits in the wallrocks of the rare-metal granites, making it possible to compare magmatic and hydrothermal REE signatures directly. The main conclusions of these studies can be summarized as follows.

The REE and other trace elements determined from bulk-rock samples are consistent with a common origin for the three subintrusions of the Khangilay complex, Khangilay, Orlovka and Spokojnoje. Many features of the trace-element variations in these granites are consistent with control by fractional crystallization. With increasing differentiation of the granites, the total REE contents decrease, chondrite-normalized patterns become flat, and the negative Eu anomaly becomes more prominent. SIMS analyses of melt inclusions from the late-stage units at Orlovka reveal extreme REE depletion (commonly less than 10 ppm for the sum of REE) and generally high Li contents (2000 to 5000 ppm Li). Concentrations of Nb are erratic but low (<10 to 117 ppm), which may reflect local variations in the timing of inclusion trapping *versus* fractionation of Nb-bearing minerals (columbite, microlite).

Like many highly evolved rare-metal granites worldwide, the granites of the Khangilay complex, and especially the satellite intrusions Spokojnoje and Orlovka, show lanthanide tetrad effects in chondrite-normalized REE diagrams. The tetrad effect is insignificant in the deepest and least-evolved units of the intrusions, and it becomes increasingly prominent upward in the sequence. The tetrad effect is developed in whole-rock samples, in associated fluorite and, most importantly, in trapped melt-inclusions.

Although melt-inclusion data prove that the lanthanide tetrad effect is developed at the magmatic stage, the process involved is not simple crystal–melt partitioning and fractionation. This was a finding in previous studies (Irber 1999) and is supported by our observation of close correlations between the degree of tetrad development and deviation from normal magmatic ratios of geochemical twin elements Y and Ho, and Zr and Hf. The levels in the Orlovka intrusion at which the tetrad effect first develops show unusual textures (snowball quartz) suggesting fluid exsolution. The common explanation for the tetrad effect by selective REE-complexing in fluids would imply that hydrothermal fluorite associated with the granites should have complementary REE patterns, but this is not observed. Hydrothermal fluorite from endogreisen in both the Orlovka and Spokojnoje granites has a REE pattern similar to that in magmatic fluorite, but with much lower REE abundances. Fluorite from exocontact veins and greisens has low REE contents and variable patterns, none of which are complementary with respect to the observed tetrad effect.

We suggest that the tetrad effect and abnormal Y/Ho or Zr/Hf values seen in this and other highly evolved F-rich granites are due to unmixing, at the magmatic stage, of a F-rich immiscible liquid (hydrosaline melt). Recent experimental studies with immiscible silicate and F-rich hydrosaline melts predict that two-liquid partitioning will produce the features observed in residual silicate melts (strong REE depletion, M-tetrads, low Y/Ho, and low Zr/Hf). However, confirmation at Orlovka of the hydrosaline melt or its crystallization products, with high REE abundance and a complementary "W-shaped" tetrad pattern, has yet to be found, even in fluorite from the endo- and exocontact hydrothermal zones. The same observation was made by Monecke *et al.* (2002) for granite-related hydrothermal fluorite in the German Erzgebirge. Indeed, despite many studies of hydrothermal fluorite from igneous and low-temperature settings (Grappin *et al.* 1979, Strong *et al.* 1984, Jebrak *et al.* 1985, Constantopoulos 1988, Ivanova *et al.* 1995, Bau & Dulski 1995, Möller 1991, 1998, Kempe & Goldstein 1997, Sallet *et al.* 2000, Kuprianova *et al.* 2002, Bühn *et al.* 2003), to our knowledge no good examples of W-shaped REE tetrads have been described in the literature.

The rarity of conjugate tetrad effects in granite-related hydrothermal aureoles is all the more enigmatic because the "M-shaped" tetrad effect is so common in evolved granites worldwide that it must reflect a widespread process in such systems. We suggest that this process is separation of a magmatic hydrosaline melt, but are forced to conclude that it rarely survives in the geologic record.

Acknowledgements

The Khangilay research in St. Petersburg has been made possible by financial support of the Russian–American Program of Basic Research and Higher Education (BRHE) and CRDF (grant Y2–G–15–03). The first author gratefully acknowledges a visiting scientist stipend from the GeoForschungsZentrum Potsdam to carry out the melt-inclusion study. For their expert help with sample preparation and microbeam analyses in Potsdam, we thank Gerhard Berger, Dieter Rhede, Oona Appelt and Ilona Schäpan. Our thanks also go to Rainer Thomas, Peter Möller and Anette Meixner for discussions and ideas about melts, fluids, fluorite and mineralized granites. Reviews by David Dolejš, Bob Linnen and Jonathan Price are gratefully acknowledged.

References

Audétat, A., Günther, D. & Heinrich, C.A. (2000): Magmatic-hydrothermal evolution in a fractionating granite: a microchemical study of the Sn–W–F-mineralized Mole Granite (Australia). *Geochim. Cosmochim. Acta* **64**, 3373-3393.

Badanina, E.V., Veksler, I.V., Thomas, R., Syritso, L.F. & Trumbull, R.B. (2004): Magmatic evolution of Li–F, rare-metal granites: a case study of melt inclusions in the Khangilay complex, eastern Transbaikalia (Russia). *Chem. Geol.* **210**, 113-133.

Bailey, J.C. (1977): Fluorine in granitic rocks and melts: a review. *Chem. Geol.* **19**, 1-42.

Bau, M. (1996): Controls on the fractionation of isovalent trace elements in magmatic and aqueous systems: evidence from Y/Ho, Zr/Hf, and lanthanide tetrad effect. *Contrib. Mineral. Petrol.* **123**, 323-333.

Bau, M. (1997): The lanthanide tetrad effect in highly evolved felsic igneous rocks – a reply to the comment by Y. Pan. *Contrib. Mineral. Petrol.* **128**, 409-412.

Bau, M. & Dulski, P. (1995): Comparative study of yttrium and rare-earth element behaviours in fluorine-rich hydrothermal fluids. *Contrib. Mineral. Petrol.* **119**, 213-223.

Bau, M., Romer, R.L., Lüders, V. & Dulski, P. (2003): Tracing element sources of hydrothermal mineral deposits: REE and Y distribution and Sr–Nd–Pb isotopes in fluorite from MVT deposits in the Pennine Orefield, England. *Mineral. Deposita* **38**, 992-1008.

Beskin, S.M., Grebennikov, A.M. & Matias, V.V. (1994): The Khangilay granite pluton and related Orlovka tantalum deposit, Transbaikalia. *Petrologya* **2**, 68-87.

Beus, A.A. (1982): Metallogeny of Precambrian rare-metal granitoids. *Rev. Bras. Geosci.* **12**, 410-413.

Bühn, B., Schneider, J., Dulski, P. & Rankin, A.H. (2003): Fluid–rock interaction during progressive migration of carbonatitic fluids, derived from small-scale trace element and Sr, Pb isotope distibution in hydrothermal fluorite. *Geochim. Cosmochim Acta* **67**, 4577-4595.

Burnham, C.W. (1976): Magmas and hydrothermal fluids. *In* Geochemistry of Hydrothermal Ore Deposits (H.L. Barnes, ed.). Wiley Interscience, New York, N.Y.

Candela, P.A. (1990): Theoretical constraints on the chemistry of the magmatic aqueous phase. *In* Ore-Bearing Granite Systems (H.J. Stein & J.L. Hannah, eds.). *Geol. Soc. Am., Spec. Pap.* **246**, 11-20.

Černý, P. (1982): Petrogenesis of granitic pegmatites. *In* Granitic Pegmatites in Science and Industry (P. Černý, ed.). *Mineral. Assoc. Can., Short Course Handbook* **8**, 293-328.

Constantopoulos, J. (1988): Fluid inclusions and rare earth element geochemistry of fluorite from south-central Idaho. *Econ. Geol.* **83**, 626-636.

Dolejš, D. & Baker, D.R. (2004): Thermodynamic analysis of the system Na_2O–K_2O–CaO–Al_2O_3–SiO_2–H_2O–F_2O_{-1}: stability of fluorine-bearing minerals in felsic igneous suites. *Contrib. Mineral. Petrol.* **146**, 762-778.

Dolejš, D. & Stemprok, M. (2001): Magmatic and hydrothermal evolution of Li–F granite: Cínovec and Krásno intrusions, Krušné hory batholith, Czech Republic. *Bull. Czech. Geol. Surv.* **76**, 77-99.

Dulski, P. (1994): Interference of oxide, hydroxide and chloride analyte species in the determination of rare earth elements in geological samples by inductively coupled plasma – mass spectrometry. *Fresenius J. Anal. Chem.* **350**, 194-203.

Dulski, P. (2001): Reference materials for geochemical studies: new analytical data by ICP–MS and critical discussion of reference values. *Geostandards Newslett., J. Geostandards Geoanal.* **25**, 87-125.

Grappin, C., Treuil, M., Yaman, S. & Touray, J.C. (1979): Le spectre des terres rares de la fluorine en tant que marqueur des propriétés du milieu de dépôt et des interactions entre solutions minéralisantes et roches sources. Exemple pris dans le District de la Marche Occidentale (France). *Mineral. Deposita* **14**, 297-309.

Helba, H., Trumbull, R.B., Morteani, G., Khalil, S.O. & Arlsan, A. (1997): Geochemical and petrographic studies of Ta mineralization in the Nuweibi albite granite complex, Eastern Desert, Egypt. *Mineral. Deposita* **32**, 164-179.

Irber, W. (1999): The lanthanide tetrad effect and its correlation with K/Rb, Eu/Eu*, Sr/Eu, Y/Ho, and Zr/Hf of evolving peraluminous granite suites. *Geochim. Cosmochim. Acta* **63**, 489-508.

Ivanova, G.F., Kolesov, G.N. & Cherkasova, G.F. (1995): REE in granite, topaz and fluorite from tungsten-bearing district of Mongolia. *Geochemistry* **8**, 1157-1177 (in Russ.).

Jahns, R.H. & Burnham, C.W. (1969): Experimental studies of pegmatite genesis. I. A model for the derivation and crystallization of granitic pegmatites. *Econ. Geol.* **64**, 843-864.

Jebrak, M., Smejkal, V. & Albert, D. (1985): Rare earth and isotopic geochemistry of the fluorite–barite vein deposits

from the western Rouergue District (France). *Econ. Geol.* **80**, 2030-2034.

JOCHUM, K.P., DINGWELL, D.B., ROCHOLL, A., STOLL, B., HOFMANN, A.W. & 31 others (2000): The preparation and preliminary characterization of eight geological MPI–DING reference glasses for in-situ microanalysis. *Geostandards Newslett., J. Geostandards Geoanal.* **24**, 87-133.

KEMPE, U. & GOLDSTEIN, S. (1997): Eu anomalies, tetrad effect and HREE enrichment in fluorites from Sn deposits: evidence for two source mixing and phase separation. *J. Czech. Geol. Soc.* **42**, 37 (abstr.).

KEPPLER, H. (1993): Influence of fluorine on the enrichment of high field strength trace elements in granitic rocks. *Contrib. Mineral. Petrol.* **114**, 479-488.

KOVALENKO, V.I., KOSTITSYN, YU.A., YARMOLYUK, V.V., BUDNIKOV, S.V., KOVACH, V.P., KOTOV, A.B., SAL'NIKOVA, E.B. & ANTIPIN, V.S. (1999): Magma sources and isotope (Sr and Nd) evolution of rare-metal Li–F rare-metal granites. *Petrology* **7**, 383-409.

KUPRIANOVA, I.I., KUKUSHKINA, O.A., SHPANOV, E.P., MATIAS, V.V., NOVIKOVA, M.N. & KUVSHINOVA, K.A. (2002): REE distribution in fluorite as an indicator of geologic-genetic features of ore deposits related to various magmatic associations. *Petrology* **10**, 312-336 (in Russ.).

LINNEN, R.L. (1998): The solubility of Nb–Ta–Zr–Hf–W in granitic melts with Li and Li+F: constraints for mineralization in rare metal granites and pegmatites. *Econ. Geol.* **93**, 1013-1025.

LINNEN, R.L. & KEPPLER, H. (2002): Melt composition control of Zr/Hf fractionation in magmatic processes. *Geochim. Cosmochim. Acta* **66**, 3293-3301.

LONDON, D. (1992): The application of experimental petrology to the genesis and crystallization of granitic pegmatites. *Can. Mineral.* **30**, 499-540.

LONDON, D., HERVIG, R.L. & MORGAN, G.B., VI (1988): Melt–vapor solibilities and elemental partitioning in peraluminous granite–pegmatite systems: experimental results with Macusani glass at 200 MPa. *Contrib. Mineral. Petrol.* **99**, 360-373.

LUTH, W.C. & TUTTLE, O.F. (1969): The hydrous vapor phase in equilibrium with granite and granite magmas. *Geol. Soc. Am., Mem.* **115**, 513-548.

MARSHALL, A.S., MACDONALD, R. & HINTON, R.W. (1998): Phenocrystic fluorite in peralkaline rhyolites, Olkaria, Kenya Rift Valley. *Mineral. Mag.* **62**, 477-486.

MASUDA, A., KAWAKAMI. O., DOHMOTO, Y. & TAKENAKA, T. (1987): Lanthanide tetrad effects in nature: two mutually opposite types, W and M. *Geochem. J.* **21**, 119-124.

MÖLLER, P. (1991): REE fractionation in hydrothermal fluorite and calcite. *In* Source, Transport and Deposition of Metals (M. Pagel & J.L. Leroy, eds.). A.A.Balkema, Rotterdam, The Netherllands (91-94).

MÖLLER, P., BAU, M., DULSKI, P. & LÜDERS, V. (1998): REE and yttrium fractionation in fluorite and their bearing on fluorite formation. Proc. 9th Quad. IAGOD Symposium. E. Schweizerbart'sche Verlagsbuchhandlung, Stuttgart, Germany (575-592).

MONECKE, T., KEMPE, U., MONECKE, J., SALA, M. & WOLF, D. (2002): Tetrad effect in rare earth element distribution patterns: a method of quantification with application to rock and mineral samples from granite-related rare metal deposits. *Geochim. Cosmochim. Acta* **66**, 1185-1196.

MÜLLER, A. & SELTMANN, R. (1999): The genetic significance of snowball quartz in highly fractionated tin granites of the Krušné Hory/Erzgebirge. *In* Mineral Deposits: Processes to Processing (C.J. Stanley *et al.*, eds.). A.A. Balkema, Rotterdam, The Netherlands (409-412).

NEGREY, E.V., ZHURAVLEV, A.Z., KOVALENKO, V.I., YARMOLUK, V.V. & SHATAGIN, K.N. (1995): Isotopic (Rb–Sr, ^{18}O) studies of tantalum-bearing lithium – fluorine granite. *Dokl. Akad. Nauk* **342**, 522-525 (in Russ.).

PEARCE, N.J.G., PERKINS, W.T., WESTGATE, J.A., GORTON, M.P., JACKSON, S.E., NEAL, C.R. & CHENERY, S.P. (1997): A compilation of new and published major and trace element data for NIST SRM 610 and NIST SRM 612 glass reference materials. *Geostandards Newslett., J. Geostandards Geoanal.* **21**, 115-144.

POLLARD, P.J. (1986): Geologic characteristics and genetic problems associated with the development of granite-hosted deposits of tantalum and niobium. *In* Lanthanides, Tantalum and Niobium (P. Möller, P. Černý & F. Saupé, eds.). Springer, Berlin, Germany (240-256).

POTTS, P.J., THOMPSON, M. & WILSON, S. (2002): G-Probe-1 – an international proficiency test for microprobe laboratories – report on round 1: February 2002 (TB–1 basaltic glass). *Geostandards Newslett., J. Geostandards Geoanal.* **26**, 197-235.

PRICE, J.D., HOGAN, J.P., GILBERT, M.C., LONDON, D. & MORGAN, G.B.,VI (1999): Experimental study of titanite–fluorite equilibria in the A-type Mount Scott granite: implications for assessing F contents of felsic magmas. *Geology* **27**, 951-954.

RAIMBAULT, L., CUNEY, M., AZENCOTT, C., DUTHOU, J.L. & JORON, J.L. (1995): Geochemical evidence for a multistage magmatic genesis of Ta–Sn–Li mineralization in the granite at Beauvoir, French Massif Central. *Econ. Geol.* **90**, 548-576.

REYF, F.G., SELTMANN, R. & ZARAISKY, G.P. (2000): The role of magmatic processes in the formation of banded Li,F-enriched granites from the Orlovka tantalum deposit, Transbaikalia, Russia: microthermometric evidence. *Can. Mineral.* **38**, 915-936.

ROEDDER, E. (1992): Fluid inclusion evidence for immiscibility in magmatic differentiation. *Geochim. Cosmochim. Acta* **56**, 5-20.

SALLET, R., MORITZ, R. & FONTIGNIE, D. (2000): Fluorite $^{87}Sr/^{86}Sr$ and REE constraints on fluid–melt relations, crystallization time span and bulk D^{Sr} of evolved high-silica granites. Tabuleiro granites, Santa Catarina, Brazil. *Chem. Geol.* **164**, 81-92.

SALVI, S., FONTAN, F., MONCHOUX, P., WILLIAMS-JONES, A.E. & MOINE, B. (2000): Hydrothermal mobilization of high field strength elements in alkaline igneous systems: evidence from the Tamazeght Complex (Morocco). *Econ. Geol.* **95**, 559-576.

SALVI, S. & WILLIAMS-JONES, A.E. (1996): The role of hydrothermal processes in concentrating high-field strength elements in the Strange Lake peralkaline complex, northeastern Canada. *Geochim. Cosmochim. Acta* **60**, 1917-1932.

SCAILLET, B. & MACDONALD, R. (2001): Phase relations of peralkaline silicic magmas and petrogenetic implications. *J. Petrol.* **42**, 825-845.

SCAILLET, B. & MACDONALD, R. (2004): Fluorite stability in silicic magmas. *Contrib. Mineral. Petrol.* **147**, 319-329.

SCHWARTZ, M.O. (1992): Geochemical criteria for distinguishing magmatic and metasomatic albite-enrichment in granitoids – examples from the Ta–Li Yichun (China) and the Sn–W deposit Tikus (Indonesia). *Mineral. Deposita* **27**, 101-108.

STRONG, D.F., FRYER, B.J. & KERRICH, R. (1984): Genesis of the St. Lawrence fluorspar deposits as indicated by fluid inclusion, rare earth element and isotopic data. *Econ. Geol.* **79**, 1142-1158.

SUN, S.-S. & MCDONOUGH, W.F. (1989): Chemical and isotope systematics of oceanic basalts: implications for mantle composition and processes. *In* Magmatism in the Ocean Basins (A.D. Saunders & M.J. Norry, eds.). *Geol. Soc., Spec. Publ.* **42**, 313-345.

SYRITSO, L.F. (1993): Geochemical aspects of zoning of rare-metal granite massifs. *Zap. Vser. Mineral. Obshchest.* **122**(2), 35-55 (in Russ.).

SYRITSO, L.F., TABUNS, E.V., VOLKOVA, E.V. BADANINA, E.V. & VYSOTSKII, YU.A. (2001): Model for the genesis of Li–F granites in the Orlovka massif, eastern Transbaikalia. *Petrology* **3**, 268-289.

SYRITSO, L.F., VOLKOVA, E.V., BADANINA, E.V. & ABUSHKEVICH, V.S. (2005): Specific enriched ultrapotassic trachyrhyodacites in the area of the Orlovka Li–F granites in eastern Transbaikalia and the problem of their relation to rare-metal granites. *Petrology* **13**, 95-98.

THOMAS, R., FÖRSTER, H.-J., RICKERS, K. & WEBSTER, J.D. (2005): Formation of extremely F-rich hydrous melt fractions and hydrothermal fluids during differentiation of highly-evolved tin-granite magmas: a melt/fluid inclusion study. *Contrib. Mineral. Petrol.* **148**, 582-601.

THOMAS, R., WEBSTER, J.D. & HEINRICH, W. (2000): Melt inclusions in pegmatite quartz: complete miscibility between silicate melts and hydrous fluid at low pressure. *Contrib. Mineral. Petrol.* **139**, 394-401.

VEKSLER, I.V. (2004): Liquid immiscibility and its role at the magmatic–hydrothermal transition: a summary of experimental studies. *Chem. Geol.* **210**, 7-31.

VEKSLER, I.V., DORFMAN, A.M., KAMENETSKY, M., DULSKI, P. & DINGWELL, D.B. (2005): Partitioning of lanthanides and Y between immiscible silicate and fluoride melts, fluorite and cryolite and the origin of the lanthanide tetrad effect in igneous rocks. *Geochim. Cosmochim. Acta* **69**, 2847-2868.

VEKSLER, I.V., THOMAS, R. & SCHMIDT, C. (2002): Experimental evidence of three coexisting immiscible fluids in synthetic granitic pegmatite. *Am. Mineral.* **87**, 775-779.

WEBSTER, J.D. (2004): The exsolution of magmatic hydrosaline chloride liquids. *Chem. Geol.* **210**, 33-48.

WIEDENBECK, M., ROCHOLL, A. & KOEPKE, J. (2001): Water – a source of systematic error in quantitative SIMS analyses of hydrous glasses. 11th Annual V.M. Goldschmidt Conf. (Hot Springs, Virginia), 3604.

WOOD, S.A. (1990): The aqueous geochemistry of the rare-earth elements and yttrium. 2. Theoretical predictions of speciation in hydrothermal solutions to 350°C at saturation water vapor pressure. *Chem. Geol.* **88**, 99-125.

YIN, LIN, POLLARD, P.J., HU, SHOUXI & TAYLOR, R.G. (1995): Geologic and geochemical characteristics of the Yichun Ta–Nb–Li deposit, Jiangxi Province, China. *Econ. Geol.* **90**, 577-585.

ZANVILEVICH, A.N., LITVINOVSKY, B.A. & ANDREEV, G.V. (1985): *Mongolia–Transbaikalian Alkaline Granitoid Province*. Nauka, Moscow, Russia (in Russ.).

ZHAO, ZHENHUX, XIONG, XIAOLIN, HAN, XIAODONG, WANG, YIXIAN, WANG, QIANG, BAO, ZHIWEI & JAHN, BORMING (2002): Controls on the REE tetrad effect in granites: evidence from the Qianlishan and Baerzhe granites, China. *Geochem. J.* **36**, 527-543.

Received October 25, 2004, revised manuscript accepted February 20, 2006.

TABLE A1. RELATIVE SENSITIVITY-FACTORS, WITH ESTIMATES OF EXTERNAL PRECISION AND ACCURACY, FOR SIMS ANALYSES OF REFERENCE GLASSES

Relative sensitivity-factors on NIST SRM610			NIST SRM 610		USGS-Tb-1G	
Isotope ratio	mean (n=12)	std. dev.		given	given	measured
$^{42}Ca/^{30}Si$	0.1129	0.0017	CaO	11.5	6.9	6.0
$^{93}Nb/^{30}Si$	0.0174	0.0013	Nb	419	28.0	23.0
$^{139}La/^{30}Si$	0.0177	0.0007	La	457	45.0	43.0
$^{140}Ce/^{30}Si$	0.0156	0.0007	Ce	448	90.0	81.8
$^{141}Pr/^{30}Si$	0.0186	0.0008	Pr	430	11.0	9.3
$^{145}Nd/^{30}Si$	0.0015	0.0001	Nd	431	40.0	36.8
$^{147}Sm/^{30}Si$	0.0031	0.0001	Sm	451	7.60	6.70
$^{151}Eu/^{30}Si$	0.0095	0.0004	Eu	461	1.90	3.86
$^{157}Gd/^{30}Si$	0.0042	0.0003	Gd	420	6.20	6.63
$^{159}Tb/^{30}Si$	0.0174	0.0009	Tb	443	0.80	1.05
$^{161}Dy/^{30}Si$	0.0032	0.0002	Dy	427	5.00	5.43
$^{165}Ho/^{30}Si$	0.0164	0.0009	Ho	449	1.00	0.95
$^{167}Er/^{30}Si$	0.0038	0.0002	Er	426	2.80	2.56
$^{169}Tm/^{30}Si$	0.0149	0.0009	Tm	420	0.40	0.40
$^{174}Yb/^{30}Si$	0.0046	0.0003	Yb	462	2.60	2.86
$^{175}Lu/^{30}Si$	0.0124	0.0009	Lu	435	0.40	0.43
$^{7}Li/^{30}Si$	1.1698	0.0733	Li	485	n.d.	
$^{9}Be/^{30}Si$	0.1684	0.0052	Be	466	n.d.	
$^{11}B/^{30}Si$	0.0342	0.0010	B	356	n.d.	

Values for primary reference glass NIST SRM610 are taken from Pearce *et al.* (1999), in ppm except for CaO, in wt.%.
Values for secondary reference glasses TB-1G from Potts *et al.* (2002), ALTHO-G from Jochum *et al.* (2000).
n.d.: No certified values are available for Li, Be and B.